

Hydrodynamics and multiscale order in confluent epithelia

Josep-Maria Armengol Collado,¹ Livio N. Carenza,¹ and Luca Giomi^{1,*}

¹*Instituut-Lorentz, Universiteit Leiden, P.O. Box 9506, 2300 RA Leiden, The Netherlands*

We formulate a hydrodynamic theory of confluent epithelia: i.e. monolayers of epithelial cells adhering to each other without gaps. Taking advantage of recent progresses toward establishing a general hydrodynamic theory of p -atic liquid crystals, we demonstrate that collectively migrating epithelia feature both nematic (i.e. $p = 2$) and hexatic (i.e. $p = 6$) order, with the former being dominant at large and the latter at small length scales. Such a remarkable multiscale liquid crystal order leaves a distinct signature in the system's structure factor, which exhibits two different power law scaling regimes, reflecting both the hexagonal geometry of small cells clusters, as well as the uniaxial structure of the global cellular flow. We support these analytical predictions with two different cell-resolved models of epithelia – i.e. the self-propelled Voronoi model and the multiphase field model – and highlight how momentum dissipation and noise influence the range of fluctuations at small length scales, thereby affecting the degree of cooperativity between cells. Our construction provides a theoretical framework to conceptualize the recent observation of multiscale order in layers of Madin-Darby canine kidney cells and pave the way for further theoretical developments.

INTRODUCTION

Collective cell migration – that is, the ability of multicellular systems to cooperatively flow, even in the absence of a central control mechanism – has surged, in the past decade, as one of the central questions in cell biology and tissue biophysics [1]. Whether spreading on a synthetic substrate [2] or invading the extracellular matrix (ECM) [3], multicellular systems can move coherently within their micro-environment and coordinate the dynamics of their actin cytoskeleton, while retaining cell-cell contacts. This ability lies at the heart of a myriad of processes that are instrumental for life, such as embryonic morphogenesis and wound healing, but also of life-threatening conditions, such as metastatic cancer.

Understanding the physical origin of this behavior inevitably demands reliable theoretical models, aimed at providing a conceptual framework for dissecting and deciphering the wealth of biophysical data stemming from *in vitro* experiments and *in vivo* observations. Following the pioneering works by [4–8] and others [9–12], *cell-resolved* models have played so far the leading role in this endeavour. Taking inspiration from the physics of foams [13, 14], these models portray a confluent tissue as a collection of adjacent or overlapping polygonal cells (Fig. 1a,b), whose dynamics is assumed to be governed by a set of overdamped Langevin equations, expressing the interplay between cells' autonomous motion and remodelling events, which change the local topology of the cellular networks.

Despite their conceptual simplicity, cell-resolved models agree remarkably well with experimental data on confluent monolayers [15, 16]. In particular they account for a solid-to-liquid transition controlled by the cells velocity and their compliance to deformations [7, 8, 11]. Furthermore, as demonstrated by Pica Ciamarra and coworkers, the solid and isotropic liquid states of these model-epithelia are separated by an intermediate *hexatic* phase,

in which the system exhibits the typical 6-fold rotational symmetry of two-dimensional crystals and yet is able to flow [17, 18]. Shortly after discovery, the same property has been recovered within the framework of the cellular Potts model, thereby strengthening the idea that hexatic order may in fact serve as a guiding principle to unravel the collective dynamics of confluent epithelia [19]. Furthermore, recent *in vitro* studies of Madin-Darby canine kidney (MDCK) cell layers demonstrated that epithelial layers can in fact feature both nematic and hexatic order, with the former being dominant at large and the latter at short length scales (see Fig. 1a,b and [20, 21]). This remarkable example of physical organization in biological matter, referred to as multiscale *hexanematic* order in [20], is believed to complement the complex network or regulatory pathways available to individual cells to achieve multicellular organization and select specific scale-dependent collective migration strategies.

Motivated by these recent discoveries, in this article we propose a continuum theory of confluent epithelia rooted in the hydrodynamics of liquid crystals with generic p -atic rotational symmetry (hereafter p -atic liquid crystals). Previous theories of epithelial hydrodynamics can be schematically grouped in two categories: 1) models based on (isotropic/polar/nematic) active gels [22–24]; 2) models built around the so called shape tensor [25–28], i.e. a rank-2 tensor, similar to the inertia tensor in kinematics, that embodies the geometrical structure of the polygonal cells. Although both classes of models hold great heuristic value and represent a solid foundation for any future development, they suffer from the same limitation: being based on a tensorial order parameter whose rank is two or less, they can account at most for 2-fold rotational symmetry (i.e. nematic order), while leaving the small scale hexatic order unresolved. To overcome this limitation, here we exploit recent advances towards extending the classic hydrodynamic theory of hexatic liquid crystals [29, 30] to account for arbitrary p -fold ro-

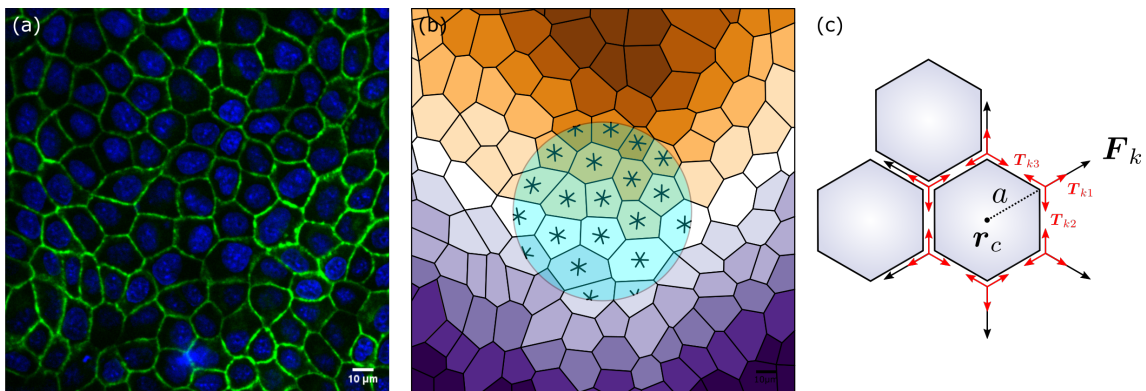


FIG. 1: (a) Example of multiscale hexanematic order in an *in vitro* layer of MDCK cells (b) and its computer-constructed segmentation. Both panels are adapted from Fig. 3 of [20]. The six-legged stars in the shaded region denote the 6-fold orientation of the cells obtained using the approach summarized in the SI. The colored stripes mark the configuration of the nematic director at the length scale of the light-blue disk. (c) Schematic representation of the 6-fold symmetric force complex exerted by cells. The red arrows indicate the structure of the contractile forces acting within the cellular junctions.

tational symmetry order [31, 32], with $p = 2$ and $p = 6$ being the most relevant cases (but possibly not the only) in the context of epithelial dynamics. We demonstrate that multiscale order is inherent to *active* liquid crystals with coupled order parameters, because of the indissoluble connection between shape and forces characterizing this class of non-equilibrium systems. Using fluctuating hydrodynamics, we explicitly compute the structure factor of epithelial layers and unveil a fascinating interplay

between the nature of momentum dissipation (i.e. viscosity or friction) and noise at short length scales, where hexatic order is dominant. Such a mechanism profoundly affects the range of density fluctuations and could be harnessed to control the degree of collectiveness of cellular motion. Finally, by testing predictions against two different microscopic models of epithelia we demonstrate the robustness of multiscale hexanematic order across the rich landscape of models of epithelia.

RESULTS AND DISCUSSION

The model

Two-dimensional p -atic liquid crystals are traditionally described in terms of the orientation field $\psi_p = e^{ip\vartheta}$, with ϑ the local orientation of the p -fold mesogens. A more general approach, proposed in [31, 32] and especially suited for hydrodynamics, revolves instead around the rank- p tensor order parameter, $\mathbf{Q}_p = Q_{i_1 i_2 \dots i_p} \mathbf{e}_{i_1} \otimes \mathbf{e}_{i_2} \otimes \dots \otimes \mathbf{e}_{i_p}$ with $i_n = \{x, y\}$ and $n = 1, 2 \dots p$, constructed upon averaging the p -th tensorial power of the local orientation $\boldsymbol{\nu} = \cos \vartheta \mathbf{e}_x + \sin \vartheta \mathbf{e}_y$. That is

$$\mathbf{Q}_p = \sqrt{2^{p-2}} \langle \langle \boldsymbol{\nu}^{\otimes p} \rangle \rangle = \sqrt{2^{p-2}} |\Psi_p| \langle \langle \mathbf{n}^{\otimes p} \rangle \rangle, \quad (1)$$

where $\langle \dots \rangle$ denotes the ensemble average and the operator $\langle \langle \dots \rangle \rangle$ has the effect of rendering an arbitrary tensor traceless and symmetric [33]. The vector $\mathbf{n} = \cos \theta \mathbf{e}_x + \sin \theta \mathbf{e}_y$ is the analogue of the director field in standard lexicon of nematic liquid crystals and marks the average cellular direction, which in turn is invariant under rotations of $2\pi/p$. The fields $|\Psi_p|$ and θ represent respectively the magnitude and phase of the complex p -atic order parameter $\Psi_p = \langle \psi_p \rangle$, while the normalization factor is chosen so that $|\mathbf{Q}_p|^2 = |\Psi_p|^2/2$ for all p values.

For $p = 2$, Eq. (1) readily gives the standard nematic order parameter tensor: i.e. $\mathbf{Q}_2 = |\Psi_2|(\mathbf{n} \otimes \mathbf{n} - \mathbb{1}/2)$, with $\mathbb{1}$ the identity tensor. In practice, if a cell's planar projection consists of a regular p -sided polygon, the microscopic orientation ϑ equates that of any of the vertices of the polygon. In the more realistic case of an *irregular* polygon, on the other hand, ϑ is given by the phase of the complex function γ_p , arising from the p -fold generalization of the classic *shape tensor* [34]. This function was introduced in [20] and is reviewed in the SI for sake of completeness.

The order parameter tensor \mathbf{Q}_p , the mass density ρ and the momentum density $\rho \mathbf{v}$, with \mathbf{v} the local velocity field, comprise the set of hydrodynamic variables describing the dynamics of a generic p -atic fluid, which in turn is governed by the following set of partial differential equations [31, 32]:

$$\frac{D\rho}{Dt} + \rho \nabla \cdot \mathbf{v} = (k_d - k_a) \rho, \quad (2a)$$

$$\rho \frac{D\mathbf{v}}{Dt} = \nabla \cdot \boldsymbol{\sigma} + \mathbf{f}, \quad (2b)$$

$$\frac{D\mathbf{Q}_p}{Dt} = \Gamma_p \mathbf{H}_p + p \langle \langle \mathbf{Q}_p \cdot \boldsymbol{\omega} \rangle \rangle + \bar{\lambda}_p \text{tr}(\mathbf{u}) \mathbf{Q}_p + \lambda_p \langle \langle \nabla^{\otimes(p-2)} \mathbf{u} \rangle \rangle + \nu_p \langle \langle \nabla^{\otimes(p \bmod 2)} \mathbf{u} \otimes [p/2] \rangle \rangle, \quad (2c)$$

where $D/Dt = \partial_t + \mathbf{v} \cdot \nabla$. Eqs. (2a) and (2b) are the mass and momentum conservation equations, with k_d and k_a rates of cell division and apoptosis, $\boldsymbol{\sigma}$ the stress tensor and \mathbf{f} an arbitrary external force per unit area. In Eq. (2c), Γ_p^{-1} is a rotational viscosity and $\mathbf{H}_p = -\delta F/\delta \mathbf{Q}_p$ is the molecular tensor describing the relaxation of the p -atic phase toward the minimum of the free energy F (see SI). The rank-2 tensors $\boldsymbol{\omega} = [\nabla \mathbf{v} - (\nabla \mathbf{v})^\top]/2$ and $\mathbf{u} = [\nabla \mathbf{v} + (\nabla \mathbf{v})^\top]/2$, with \top indicating transposition, are the vorticity and strain rate tensors respectively, whereas the dot product in the first line of the equation implies a contraction of one index of \mathbf{Q}_p with one of $\boldsymbol{\omega}$: i.e. $(\mathbf{Q}_p \cdot \boldsymbol{\omega})_{i_1 i_2 \dots i_p} = Q_{i_1 i_2 \dots j} \omega_{j i_p}$. On the second line $(\nabla^{\otimes n})_{i_1 i_2 \dots i_n} = \partial_{i_1} \partial_{i_2} \dots \partial_{i_n}$, while $[\dots]$ denotes the floor function and $p \bmod 2 = p - 2 \lfloor p/2 \rfloor$ is zero for even p values and one for odd p values. Finally, $\bar{\lambda}_p$, λ_p and ν_p are material parameters expressing the strength of the coupling between p -atic order and flow.

Now, in order for Eqs. (2) to account for the dynamics of epithelial cell layers, we must specify the structure of the external force \mathbf{f} in Eq. (2b) and the stress tensor $\boldsymbol{\sigma}$. As cells collectively crawl on a substrate, at a speed of order 0.1 to 1 $\mu\text{m}/\text{min}$ [35, 36], the former can be model as a Stokesian drag: $\mathbf{f} = -\zeta \mathbf{v}$, with ζ a drag coefficient. A more realistic treatment of the interplay between the cells and the substrate would account for the traction forces exerted by the cells' cryptic lamellipodium as well as for the compliance of the substrate [37] and will be considered in the future. The stress tensor, on the other hand, is routinely decomposed into a passive and an active component: i.e. $\boldsymbol{\sigma} = \boldsymbol{\sigma}^{(p)} + \boldsymbol{\sigma}^{(a)}$. The passive stress tensor is in turn expressed as $\boldsymbol{\sigma}^{(p)} = -P \mathbb{1} + \boldsymbol{\sigma}^{(e)} + \boldsymbol{\sigma}^{(r)} + \boldsymbol{\sigma}^{(v)}$, where P is the pressure, $\boldsymbol{\sigma}^{(e)}$ is the *elastic* stress, arising in response of a static deformation of a fluid patch, and $\boldsymbol{\sigma}^{(r)}$ and $\boldsymbol{\sigma}^{(v)}$ are respectively the *reactive* (i.e. energy preserving) and *viscous* (i.e. energy dissipating) stresses originating from the reversible and irreversible couplings between p -atic order and flow. The generic expression of $\boldsymbol{\sigma}^{(p)}$ was derived in [31, 32] and is reported in the Supplementary information.

The active stress $\boldsymbol{\sigma}^{(a)}$, on the other hand, can be constructed phenomenologically for arbitrary p values in the form

$$\boldsymbol{\sigma}^{(a)} = \sum_p \left(\alpha_p \nabla^{\otimes(p-2)} \odot \mathbf{Q}_p + \beta_p \llbracket \nabla^{\otimes 2} |\mathbf{Q}_p|^2 \rrbracket \right), \quad (3)$$

where the symbol \odot denotes a contraction of all matching indices of the two operands and yields a tensor whose rank equates the number of unmatched indices: i.e. letting \mathbf{A}_p and \mathbf{B}_q be two generic tensors of rank $p < q$, then $(\mathbf{A}_p \odot \mathbf{B}_q)_{i_1 i_2 \dots i_{q-p}} = A_{j_1 j_2 \dots j_p} B_{j_1 j_2 \dots j_p i_1 i_2 \dots i_{q-p}}$. The sum over p , finally, reflects the possibility of having not only one, but multiple types of p -atic order coexisting within the same system, as experiments on *in vitro* layers of MDCK cells have recently suggested [20, 21].

Before exploring the consequences of the latter assumption, some comment about the physical interpretation of the terms featured in Eq. (3) is in order. The first term on the right-hand side of Eq. (3) is the stress resulting from the contractile or extensile forces exerted at the length scale of individual cells. To illustrate this concept one can assume each cell to exert a p -fold symmetric force complex: i.e. $\mathbf{F}_c = \sum_{k=1}^p \mathbf{F}_k \delta(\mathbf{r} - \mathbf{r}_c - a \boldsymbol{\nu}_k)$ with \mathbf{F}_k the force exerted by a cell at each vertex and originating from the imbalance of the tensions \mathbf{T}_{kl} , driven by the active contraction of the cellular junctions, converging at the k -th vertex: i.e. $\mathbf{F}_k = \sum_l \mathbf{T}_{kl}$ (see Fig. 1c). The quantities \mathbf{r}_c and a are the cell's centroid and circumradius respectively, while $\boldsymbol{\nu}_k = \cos(\vartheta + 2\pi k/p) \mathbf{e}_x + \sin(\vartheta + 2\pi k/p) \mathbf{e}_y$. We stress that, while the individual tensions acting along the junctions are exclusively contractile, the resulting vertex forces can be either contractile (i.e. $\mathbf{F}_k \cdot \boldsymbol{\nu}_k < 0$) or extensile ($\mathbf{F}_k \cdot \boldsymbol{\nu}_k > 0$), depending on the overall tension distribution and the geometry of the cellular network. Next, assuming $\mathbf{F}_k = f \boldsymbol{\nu}_k$ and expanding the delta function about $a = 0$ yields $\mathbf{F}_c = \sum_{m=0}^{\infty} \mathbf{f}_m$, where

$$\mathbf{f}_m = \nabla^{\otimes m} \odot \left[\frac{(-a)^m f}{m!} \left(\sum_{k=1}^p \boldsymbol{\nu}_k^{\otimes(m+1)} \right) \delta(\mathbf{r} - \mathbf{r}_c) \right]. \quad (4)$$

Because of the p -fold symmetry of the force complex $\mathbf{f}_m = \mathbf{0}$ for all even m values, unless $m = p - 1$, whereas odd m values yields, up to symmetrization, $\sum_{k=1}^p \boldsymbol{\nu}_k^{\otimes(m+1)} \sim \mathbb{1}^{\otimes(m+1)/2}$. Thus, after some algebraic manipulation, one finds $\mathbf{F}_c \approx -apf/2 \nabla[(1 + a^2/8 \nabla^2 + \dots) \delta(\mathbf{r} - \mathbf{r}_c)] + \mathbf{f}_{p-1}$. Finally, taking $\langle \sum_c \mathbf{F}_c \rangle = -P^{(a)} \mathbb{1} + \boldsymbol{\sigma}^{(a)}$ gives the following expression for contributions to the pressure and the deviatoric stress resulting from the active expansion and contraction of the cells. That is

$$P^{(a)} = \frac{apf}{2} \left(n + \frac{a^2}{8} \nabla^2 n + \dots \right), \quad (5a)$$

$$\boldsymbol{\sigma}^{(a)} = \frac{(-a)^{p-1} p n f}{\sqrt{2^{p-2}} (p-1)!} \nabla^{\otimes(p-2)} \odot \mathbf{Q}_p, \quad (5b)$$

where $n = \langle \sum_c \delta(\mathbf{r} - \mathbf{r}_c) \rangle$ is the cell number density. From Eq. (5b), one finds the following expression for the phenomenological parameter α_p in Eq. (3): i.e. $\alpha_p = (-a)^{p-1} p n f / [\sqrt{2^{p-2}} (p-1)!]$. Notice that both constants a and f involved in Eqs. (5) are, in general, order-dependent. We will come back on this aspect in the Conclusion section.

The second term in Eq. (3), by contrast, expresses the active stress resulting from the spatial variations of the p -atic order parameter and, although similar to other contributions to the passive stress $\boldsymbol{\sigma}^{(p)}$, cannot be derived from equilibrium considerations. Other terms constructed by contracting \mathbf{Q}_p with $\nabla^{\otimes 2}$ can be expressed as linear combinations of this and $\boldsymbol{\sigma}^{(p)}$, thus

lead to a mere renormalization of the material parameters. It must be noted that the stress tensor enters in Eq. (2b) only via its divergence. Thus, possible second order active terms such as $Q_{k_1 k_2 \dots k_p} \partial_i \partial_j Q_{k_1 k_2 \dots k_p}$, $Q_{ij k_3 \dots k_p} \partial_{l_1} \partial_{l_2} Q_{l_1 l_2 k_3 \dots k_p}$ etc., are mechanically equivalent to the terms $\partial_i Q_{k_1 k_2 \dots k_p} \partial_j Q_{k_1 k_2 \dots k_p}$ and $Q_{k_1 k_2 \dots i} H_{k_1 k_2 \dots j} - H_{k_1 k_2 \dots i} Q_{k_1 k_2 \dots j}$ arising from the passive stresses, as both sets of terms lead to the same body forces.

We observe that Eq. (3) already entails a multiscale hydrodynamic behavior even when a single p value is considered. Such a crossover is expected at length scales larger than $\ell = (\alpha_p/\beta_p)^{1/(p-4)}$, where the second term of the right-hand side of Eq. (3) overweights the first term, reflecting the p -fold symmetry of the local active forces. In the presence of multiple types of p -atic order, the p -dependent structure of the active stress renders the multiscale nature of the system enormously more dramatic. To illustrate this crucial point, here we postulate the system to behave as a hexanematic liquid crystal. Formally, such a scenario can be accounted by simultaneously solving two variants of Eq. (2c), for \mathbf{Q}_2 and \mathbf{Q}_6 . In turn, the interplay between nematic and hexatic order results from a combination of dynamical and energetic effects. The former arise from active flow, which affects the local configuration of both tensor order parameters via the last four terms in Eq. (2c). The latter, instead, can be embedded into the free energy $F = \int dA (f_2 + f_6 + f_{2,6})$, where

$$f_p = \frac{1}{2} L_p |\nabla \mathbf{Q}_p|^2 + \frac{1}{2} A_p |\mathbf{Q}_p|^2 + \frac{1}{4} B_p |\mathbf{Q}_p|^4, \quad (6a)$$

$$f_{2,6} = \kappa_{2,6} |\mathbf{Q}_2|^2 |\mathbf{Q}_6|^2 + \chi_{2,6} \mathbf{Q}_2^{\otimes 3} \odot \mathbf{Q}_6. \quad (6b)$$

Here, A_p and B_p are constants setting the magnitude of the order parameter at the length scale of the short distance cut-off, here assumed to be of the order of the cell size, and $\kappa_{2,6}$ determines the extent to which the magnitude of the hexatic order parameter is influenced by that of the nematic order parameter and vice versa. The constant $\chi_{2,6}$, on the other hand, is analogous to an inherent susceptibility, expressing the propensity of the nematic and hexatic directors towards mutual alignment. The free energy contribution $f_{2,6}$ can further be augmented with several additional terms of higher differential order: e.g. $(\mathbf{Q}_2 \odot \nabla \mathbf{Q}_2) \cdot (\mathbf{Q}_6 \odot \nabla \mathbf{Q}_6)$, $|\nabla(\mathbf{Q}_2^{\otimes 3} \odot \mathbf{Q}_6)|^2$, $\nabla^2(\mathbf{Q}_2^{\otimes 3} \odot \mathbf{Q}_6)$ etc. For simplicity, here we ignore these and higher order couplings and focus on the zeroth order terms included in Eq. (6b).

Crucially, Eqs. (3) and (6) entail two length scales, reflecting the distance at which the passive torques originating from the entropic elasticity of the nematic and hexatic phases counterbalance those arising from the active stresses:

$$\ell_2 = \sqrt{\frac{L_2}{|\alpha_2|}}, \quad \ell_6 = \sqrt{\frac{|\alpha_6|}{L_6}}. \quad (7)$$

The former is the well known active nematic length scale, dictating both the hydrodynamic stability [38] and the large scale structure of spatiotemporal chaos in active nematics [39] and whose signature in multicellular systems has been identified in both eukaryotes [40] and prokaryotes [41]. The latter, on the other hand, sets the typical size of hexatic domains at the small length scale. Remarkably, ℓ_2 and ℓ_6 inversely depend on the magnitude of cellular forces [see Eqs. (5)]. Thus, increasing activity has the effect of collapsing the multiscale structure of the system towards a single length scale, where $\ell_2 \approx \ell_6$. Two additional length scales, of purely passive nature, originate from the competition between rotational diffusion and the ordering dynamics driven by either liquid crystalline structure on the other one. These are given by $\ell_{\chi,2} = \sqrt{L_2/\chi_{2,6}}$ and $\ell_{\chi,6} = \sqrt{L_6/\chi_{2,6}}$. Their role will be discussed in the following section, in the framework of fluctuating hydrodynamics.

Finally, in the passive limit, when $\alpha_2 = 0$ and $\alpha_6 = 0$, Eqs. (2) and (6) reduce to those of a two-dimensional liquid crystal with coupled nematic and hexatic order parameter. The latter can be found, e.g., in free-standing liquid hexatic films [42, 43], where molecules are either orthogonal to the mid-surface of the film or tilted by a fixed angle. In the latter case, the projection of the average molecular direction on the tangent plane of the mid-surface gives rise to in-plane nematic order, which is coupled to the 6-fold *bond*-orientational order associated with the underlying hexatic phase [see, e.g., [44–46] for a theoretical account and [47] for recent developments]. As we will detail in the following, activity profoundly alters this scenario by acting as a mechanical bandpass filter, which renders hexatic order *dominant* at length scales $\ell \ll \ell_6$ and nematic order at length scales $\ell \gg \ell_2$. We stress that by dominant, here we intend able to drive morphological features, dynamical behaviors, and fluctuations reflecting the underlying orientational order. At intermediate length scales, i.e. $\ell_6 \ll \ell \ll \ell_2$, there is no dominant order and the system's collective behavior is determined by the complex interplay of competing active and passive effects. To make progress, here we focus on the most dramatic hexatic- and nematic-dominated behaviors and treat intermediate length scales as simply as possible.

Multiscale order in epithelia

To elucidate the multiscale organization of the system, we next compute the structure factor $S(|\mathbf{q}|)$, using the classic framework of fluctuating hydrodynamics [see, e.g., [48]]. To this end, we assume both the nematic and the hexatic scalar order parameters to be uniform throughout the system and set $k_d = k_a$ and $\lambda_p = 0$ for simplicity. We stress that the validity of this approximation is strictly related with the present comparison between the

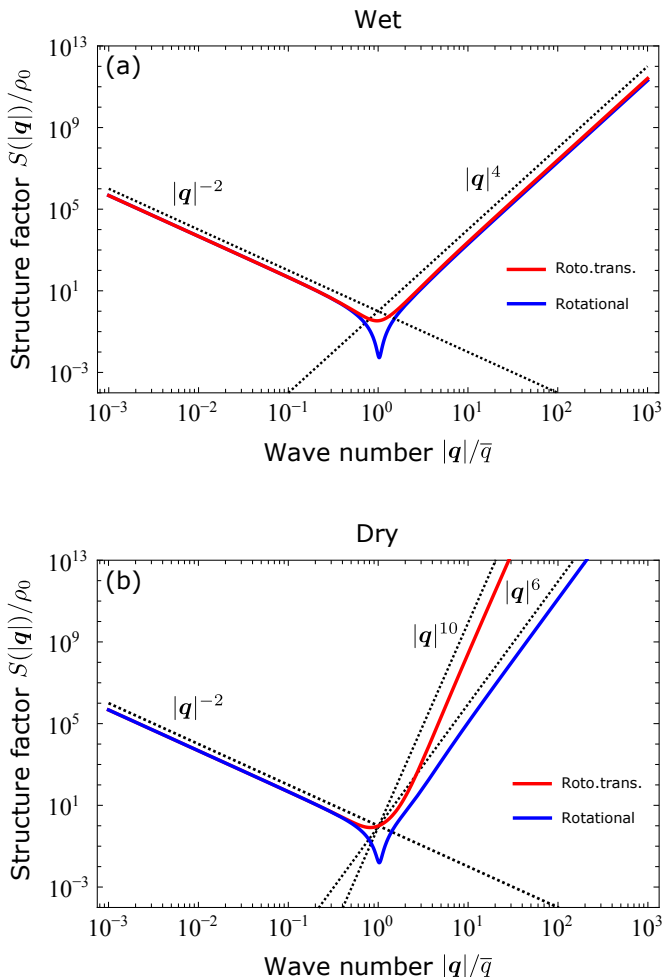


FIG. 2: Structure factor $S(|\mathbf{q}|)$ obtained from the analytical solutions of the linearized hydrodynamic equations in the presence of two different noise fields: purely rotational (blue) and rototranslational (red). The full analytical expression of $S(|\mathbf{q}|)$ is given in the SI, together with a derivation of the exact asymptotic expansions of Eq. (8). (a) As long as viscous dissipation takes place (i.e. “wet” regime), $S(|\mathbf{q}|) \sim |\mathbf{q}|^4$ in the limit $|\mathbf{q}| \rightarrow \infty$, irrespective of the type of noise. (b) On the other hand, when friction is the sole momentum dissipation mechanism at play (“dry” regime), $S(|\mathbf{q}|) \sim |\mathbf{q}|^6$ in case of rotational noise and $S(|\mathbf{q}|) \sim |\mathbf{q}|^{10}$ when noise is both rotational and translational. In both panels the wave number $|\mathbf{q}|$ is rescaled by $\bar{q} = 2\pi/\bar{\ell}$, with $\bar{\ell} = (\ell_2 + \ell_6)/2$ and ℓ_2 and ℓ_6 as defined in Eq. (7).

hydrodynamic theory presented in this article and cell-resolved models. An assessment of the relevance of this and the other material parameters featured in Eqs. (2) can only be achieved via experimental scrutiny and is likely to depend on the specific cell type and environmental conditions. Furthermore, as the typical Reynolds number of collective epithelial flow is in the range 10^{-7} – 10^{-6} , we neglect inertial effects: i.e. $\rho D\mathbf{v}/Dt = 0$. With these simplifications, whose legitimacy will be assessed *a posteriori*, one can reduce Eqs. (2) to three coupled dif-

ferential equations for the density and the phases of the hexatic and nematic order parameter tensors (see SI). These equations, in turn, can be linearized about the trivial configuration, where all fields are spatially uniform and $\mathbf{v} = \mathbf{0}$, and augmented with noise terms to give the following *exact* asymptotic expansion

$$S(|\mathbf{q}|) \sim \frac{s_{-2}}{|\mathbf{q}|^2} + s_\beta |\mathbf{q}|^\beta. \quad (8)$$

The first term entails the typical giant number density fluctuations associated with the active nematic behavior at the large scale, with $s_{-2} \sim \alpha_2^2$. This effect is overestimated at the linear order, leading to an inverse quadratic dependence on the wave number $|\mathbf{q}|$ [48], but is generally renormalized by nonlinearities, so that $\lim_{|\mathbf{q}| \rightarrow 0} S(|\mathbf{q}|) \sim |\mathbf{q}|^{-\alpha}$, with $1 < \alpha < 2$ [49, 50].

The second term, on the other hand, reflects the 6–fold symmetry characterizing the structure of epithelia at the small length scale, with $s_\beta \sim \alpha_6^2$ and the exponent β determined by the specific energy dissipation mechanism, as well as by the specific structure of the noise. As detailed in the Supplementary information, here we consider *four* alternative scenarios, obtained upon combining two different momentum dissipation mechanisms (i.e. viscosity and friction) with two different types of noise (i.e. rototranslational and purely rotational). In the presence of *viscous* dissipation, i.e. a regime referred to as “wet” in the jargon of active matter, $\beta = 4$ irrespective of the nature of noise. Conversely, in the “dry” limit, when the shear and bulk viscosity vanish and momentum dissipation solely results from the frictional interactions with the substrate, β differs depending on whether noise affects both cells’ orientational and translational dynamics, or only the former. Specifically, when only orientational noise is considered, $\beta = 6$. By contrast, $\beta = 10$ in the presence of *conservative* rototranslational noise. We again stress that Eq. (8) is an exact asymptotic expansion, as one could verify upon comparison with the full analytical solutions plotted in Fig. 2, and *not* a truncated power series.

To test the significance of these predictions and connect the present hydrodynamic theory with the existing literature, in Fig. 3a we compare the structure factor obtained from numerical simulations of two different cell-resolved models of epithelia – i.e. the self-propelled Voronoi model (SPV) [8] and the multiphase field model (MPF) [11] (see the insets Fig. 3b for typical configurations of the two models) – with that resulting from a numerical integration of Eqs. (2) [51, 52], with *none* of the simplifications behind Eq. (8). In both microscopic models, cells are treated as persistent random walkers, self-propelling at constant speed v_0 and whose direction of motion undergoes rotational diffusion with diffusion coefficient D_r (see SI for details). Noise is therefore expected to affect both the rotational and translational dynamics of the cell monolayer, although in a way that, unlike in

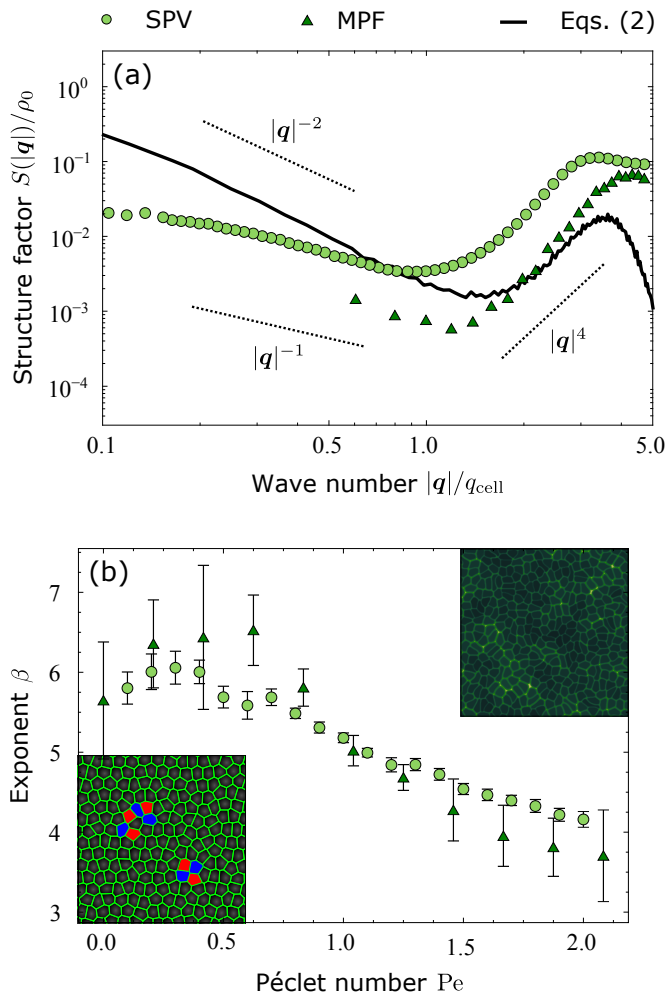


FIG. 3: (a) Structure factor of model-epithelia calculated from a numerical integration of Eqs. (2) (black line) and from simulations of two different cell-resolved models: i.e. the self-propelled Voronoi model (SPV, red) and the multiphase field model (MPF, blue), for a particular choice of parameters. The dashed diagonal lines mark the scaling regimes obtained analytically at the linear order, Eq. (8), and the wave number $|\mathbf{q}|$ is rescaled by $q_{\text{cell}} = 2\pi/\Delta x_{\text{LB}}$, where Δx_{LB} is the grid size used by the Lattice Boltzmann integrator (see SI for details). (b) The exponent β , as defined in Eq. (8), versus the Péclet number Pe , reflecting the persistence of directed cellular motion in front of diffusion. Insets: typical configurations of the SPV (bottom left) and MPF (top right) models.

our analytical treatment, cannot be trivially decoupled. Consistently with our linear analysis, both data sets exhibit two different power-law scaling regimes at small and large length scales. At small length scales, the structure factor scales like $S(|\mathbf{q}|) \sim |\mathbf{q}|^\beta$, with β monotonically decreasing from 6 to 4 upon increasing the Péclet number $Pe = \xi_0/a$ expressing the ratio between cells’ persistence length $\xi_0 = v_0/D_r$ and their typical size a (see Fig. 3b).

Conversely, at large length scales, the structure factor scales like an inverse power law, with exponent consistent with the large scale behavior of active nematics [50].

These observations can be rationalized in the light of the previous fluctuating hydrodynamic analysis. In the limit $Pe \rightarrow 0$, cells do not self-propel, noise is predominantly orientational and momentum propagates only at distances comparable to the average cell size. Under this circumstance, an *in silico* cell layer, whether modelled via the SPV or the MPF, behaves therefore as a “dry” active system subject to purely rotational noise, for which, consistently with our analysis, $\beta = 6$. Increasing Pe has the two-fold effect of converting noise from purely rotational to rototranslational and, by stimulating cooperativity in the cellular motion, to increase the range of momentum propagation, thus driving a crossover of the cell layer from “dry” to “wet”, hence from $\beta = 6$ to $\beta = 4$. The simple linear calculation, summarized in the Supplementary part, does not allow us to resolve the full crossover, but does provide a precise estimate of the upper and lower bounds. Finally, along the wet-dry crossover, viscosity must emerge from the cells’ lateral interactions. A precise understanding of this process is outside of the scope of the present work, but recent numerical work on the Vertex model has already highlighted the existence of a rich landscape of exotic rheological phenomena, resulting from the interplay between cellular motion, morphology and adhesion [53, 54]. The latter could possibly explain the non-monotonic behavior at small Pe values, as a crossover from a shear-thinning to the shear-thickening behavior [54] for additional numerical evidence of this effect).

A different signature of multiscale hexanematic order can be identified in the structure of the cross-correlation function

$$C_{26}(\mathbf{r}) = \frac{\langle \psi_2(\mathbf{r})\psi_6^*(\mathbf{0}) + \psi_2^*(\mathbf{r})\psi_6(\mathbf{0}) \rangle}{2}. \quad (9)$$

At equilibrium, and if deformations are sufficiently gentle to render backflow effects negligible, its behavior can be divided in two regimes, depending on how the distance $|\mathbf{r}|$ compares to the length scales $\ell_{\chi,2}$ and $\ell_{\chi,6}$ defined in the previous section and expressing the typical distance at which the mutual alignment rate of the hexatic and nematic orientations overcome that of rotational diffusion. In the simplest possible setting, when $\ell_{\chi,2} = \ell_{\chi,6} = \ell_\chi$, fluctuations dominate at short distances and the hexatic and nematic orientations are uncorrelated. Thus $C_{26}(\mathbf{r})$ is approximately constant for $|\mathbf{r}| \ll \ell_\chi$. The picture is reversed for $|\mathbf{r}| \gg \ell_\chi$. In this range the hexatic and nematic orientations are “locked” in a parallel configuration, i.e. $\text{Arg}(\psi_2)/2 \approx \text{Arg}(\psi_6)/6$, or tilted by $\pi/6$ with respect to each other, depending on the sign of the constant $\chi_{2,6}$, and the cross-correlation function exhibits the standard power-law decay characterizing two-dimensional liquid crystals with a single order parameter: i.e. $C_{26}(\mathbf{r}) \sim (|\mathbf{r}|/\ell_\chi)^{-\eta_{26}}$, with η_{26} a specific instance of the generic non-universal exponent $\eta_{26} = 6k_B T/(\pi K)$, with K the orientational stiffness of

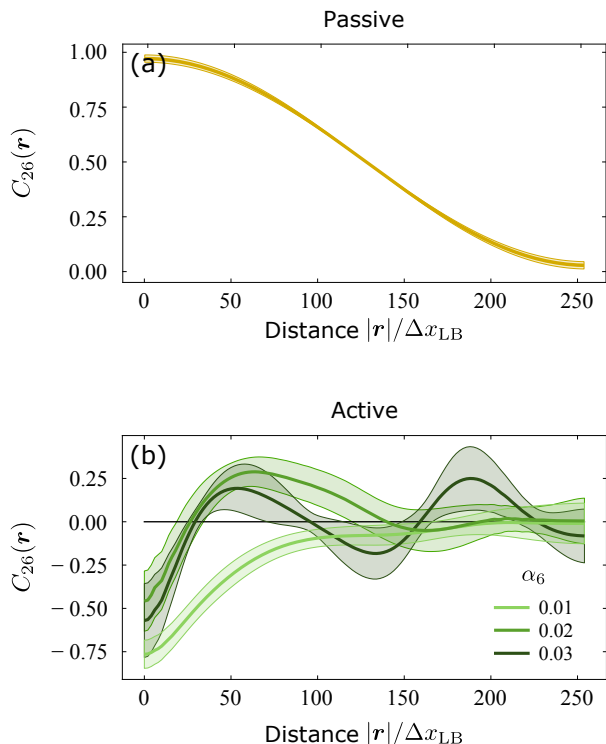


FIG. 4: Cross-correlation function $C_{26}(\mathbf{r})$, as defined in Eq. (9), obtained from a numerical integration of Eqs. (2) augmented with rotational noise. (a) In the passive case, when $\alpha_2 = 0$ and $\alpha_6 = 0$, the correlation function decays with $|\mathbf{r}|$ at a rate that is lower at short distances, where the dynamics of the hexatic and nematic orientations is dominated by fluctuations, and larger at long distances, where the orientations are “locked” in a parallel configuration, or tilted by $\pi/6$ with respect to each other. (b) In the active case, conversely, the cross-correlation function has a damped oscillatory behavior. Consistently with Eqs. (7) and the related discussion, the range of the oscillations, corresponding to the distance at which these are fully damped, increases with the hexatic activity α_6 , indicating an enhancement of hexatic order at larger length scales. Distance is expressed in terms of the grid size Δx_{LB} used by the Lattice Boltzmann integrator (see SI for details).

both phases (proportional to $L_2 = L_6$). An analytical treatment of this simple case is reported in SI. In the more generic case, in which $\ell_{\chi,2} \neq \ell_{\chi,6}$ and the relaxation rates of the hexatic and nematic phase differ, the cross-correlation function has a less standard functional form, but still features a slow and fast decay regime at short and large distances respectively. An example of such a scenario, obtained from a numerical integration of Eqs. (2) with $\alpha_2 = 0$ and $\alpha_6 = 0$, is shown in Fig. 4a. The curves in Fig. 4b correspond instead to simulated configurations of the cross-correlation function of $C_{26}(\mathbf{r})$ for finite hexatic and nematic activity. In this case, the cross-correlation function exhibits an oscillatory behavior at short distances and vanishes at a length scale that becomes progressively large as the hexatic activity is in-

creased. Consistently with our previous analysis, this latter feature confirms the existence of a hierarchy of orientationally ordered structures nested into each other at different length scales.

Taken together, our calculations of the structure factor and the cross-correlation function demonstrate that the hydrodynamic theory embodied in Eqs. (2) and (6) is able to account for the multiscale hexanematic order observed in experiments [20, 21] and harnesses it into a continuum mechanical framework. Whereas the origin of hexanematic order is still a matter of investigation, the current experimental and numerical evidence suggests that, similarly to granular materials [55], large scale nematic order could arise from the self-organization of the microscopic force hexapoles into *force chains*. The possibility of similarity between these two phenomena has also been in relation to the initial phase of *Drosophila* gastrulation, where linear arrays of cells simultaneously undergo apical constriction in the ventral furrow region [56].

CONCLUSIONS

In conclusion, we have introduced a continuum model of collectively migrating layers of epithelial cells, built upon a recent generalization of the hydrodynamic theory of p -atic liquid crystals [31, 32]. This approach allows one to account for arbitrary discrete rotational symmetries, thereby going beyond existing hydrodynamic theories of epithelia [22–28], where the algebraic structure of the hydrodynamic variables renders impossible to account for liquid crystal order other than isotropic (i.e. $p = 0$), polar (i.e. $p = 1$) or nematic (i.e. $p = 2$). Upon computing the static structure factor and comparing this with the outcome of two different cell-resolved models – i.e. the SPV [8] and MPF [11] models – we have shown that, consistently with recent experimental findings [20, 21], epithelial layers may in fact comprise both nematic and hexatic (i.e. $p = 6$) order, coexisting at different length scales. Although the consequences of such a remarkable versatility are yet to be explored, we expect hexatic order to be relevant for short-scale remodelling events, where the local nature of hexatic order, combined with the rich dynamics of hexatic defects [30, 57], may mediate processes such as cell intercalations and the rearrangement of multicellular *rosettes* [58, 59]. Such a local motion, in turn, may be coordinated at the large scale by the underlying nematic order, giving rise to a persistent unidirectional flow, such as that observed during wound healing and cancer progression [1]. Furthermore, the existence of multiscale liquid crystal order echoes the most recent understanding of phenotypic plasticity in tissues, according to which the epithelial (i.e. solid-like) and mesenchymal (i.e. liquid-like) states represent the two ends of a spectrum of intermediate phenotypes [60]. These intermediate states display distinct-

tive cellular characteristics, including adhesion, motility, stemness and, in the case of cancer cells, invasiveness, drug resistance etc. Can multiscale liquid crystal order help understanding how the biophysical properties of tissues vary along the epithelial-mesenchymal spectrum? This and related questions will be addressed in the near future.

We are indebted with Massimo Pica Ciamarra and David Nelson for insightful discussions. This work is supported by the ERC-CoG grant HexaTissue (L.N.C and L.G.) and by Netherlands Organization for Scientific Research (NWO/OCW) as part of the research program “The active matter physics of collective metastasis” with project number Science-XL 2019.022 (J.-M.A.C). Part of this work was carried out on the Dutch national e-infrastructure with the support of SURF through the Grant 2021.028 for computational time.

* giomi@lorentz.leidenuniv.nl

- [1] P. Friedl and D. Gilmour, *Nat. Rev. Mol. Cell Bio.* **10**, 445–457 (2009).
- [2] X. Serra-Picamal, V. Conte, R. Vincent, E. Anon, D. T. Tambe, E. Bazellieres, J. P. Butler, J. J. Fredberg, and X. Trepap, *Nat. Phys.* **8**, 628–634 (2012).
- [3] A. Haeger, S. Alexander, M. Vullings, F. M. P. Kaiser, C. Veelken, U. Flucke, G. E. Koehl, M. Hirschberg, M. Flentje, R. M. Hoffman, E. K. Geissler, S. Kissler, and P. Friedl, *J. Exp. Med.* **217** (1) (2020), 10.1084/jem.20181184.
- [4] H. Honda, *J. Theor. Biol.* **72**, 523 (1978).
- [5] T. Nagai and H. Honda, *Philos. Mag. B* **81**, 699 (2001).
- [6] R. Farhadifar, J.-C. Röper, B. Aigouy, S. Eaton, and F. Jülicher, *Curr. Biol.* **17**, 2095 (2007).
- [7] D. Bi, J. H. Lopez, J. M. Schwarz, and M. L. Manning, *Nat. Phys.* **11**, 1074 (2015).
- [8] D. Bi, X. Yang, M. C. Marchetti, and M. L. Manning, *Phys. Rev. X* **6**, 021011 (2016).
- [9] A. Boromand, A. Signoriello, F. Ye, C. S. O’Hern, and M. D. Shattuck, *Phys. Rev. Lett.* **121**, 248003 (2018).
- [10] R. Mueller, J. M. Yeomans, and A. Doostmohammadi, *Phys. Rev. Lett.* **122**, 048004 (2019).
- [11] B. Loewe, M. Chiang, D. Marenduzzo, and M. C. Marchetti, *Phys. Rev. Lett.* **125**, 038003 (2020).
- [12] S. Monfared, G. Ravichandran, J. E. Andrade, and A. Doostmohammadi, arXiv:2108.07657 (2021).
- [13] F. Graner, B. Dollet, C. Raufaste, and P. Marmottant, *Eur. Phys. J. E* **25**, 349 (2008).
- [14] P. Marmottant, C. Raufaste, and F. Graner, *Eur. Phys. J. E* **25**, 371 (2008).
- [15] J.-A. Park, J. H. Kim, D. Bi, J. A. Mitchel, N. T. Qazvini, K. Tantisira, C. Y. Park, M. McGill, S.-H. Kim, B. Gweon, J. Notbohm, R. J. Steward, S. Burger, S. H. Randell, A. T. Kho, D. T. Tambe, C. Hardin, S. A. Shore, E. Israel, D. A. Weitz, D. J. Tschumperlin, E. P. Henske, S. T. Weiss, M. L. Manning, J. P. Butler, J. M. Drazen, and J. J. Fredberg, *Nat. Mater.* **14**, 1040 (2015).
- [16] L. Atia, D. Bi, Y. Sharma, J. A. Mitchel, B. Gweon, S. A. Koehler, S. J. DeCamp, B. Lan, J. H. Kim, R. Hirsch, A. F. Pegoraro, K. H. Lee, J. R. Starr, D. A. Weitz, A. C. Martin, J.-A. Park, J. P. Butler, and J. J. Fredberg, *Nat. Phys.* **14**, 613–620 (2018).
- [17] Y.-W. Li and M. Pica Ciamarra, *Phys. Rev. Materials* **2**, 045602 (2018).
- [18] A. Pasupalak, Y.-W. Li, R. Ni, and M. Pica Ciamarra, *Soft Matter* **16**, 3914 (2020).
- [19] M. Durand and J. Heu, *Phys. Rev. Lett.* **123**, 188001 (2019).
- [20] J.-M. Armengol-Collado, L. N. Carenza, J. Eckert, D. Krommydas, and L. Giomi, *Nat. Phys.* (2023), 10.1038/s41567-023-02179-0.
- [21] J. Eckert, B. Ladoux, R.-M. Mège, L. Giomi, and T. Schmidt, *Nat. Commun.* **14**, 5762 (2023).
- [22] J. Ranft, M. Basan, J. Elgeti, J.-F. Joanny, J. Prost, and F. Jülicher, *Proc. Natl. Acad. Sci. U.S.A* **107**, 20863 (2010).
- [23] M. Popović, A. Nandi, M. Merkel, R. Etournay, E. S., F. Jülicher, and G. Salbreux, *New J. Phys.* **19**, 033006 (2017).
- [24] C. Pérez-González, R. Alert, C. Blanch-Mercader, M. Gómez-González, T. Kolodziej, E. Bazellieres, J. Casademunt, and X. Trepap, *Nat. Phys.* **15**, 79 (2019).
- [25] S. Ishihara, P. Marcq, and K. Sugimura, *Phys. Rev. E* **96**, 022418 (2017).
- [26] M. Czajkowski, D. Bi, M. L. Manning, and M. C. Marchetti, *Soft Matter* **14**, 5628 (2018).
- [27] A. Hernandez and M. C. Marchetti, *Phys. Rev. E* **103**, 032612 (2021).
- [28] D. Grossman and J.-F. Joanny, *Phys. Rev. Lett.* **129**, 048102 (2022).
- [29] A. Zippelius, *Phys. Rev. A* **22**, 732 (1980).
- [30] A. Zippelius, B. I. Halperin, and D. R. Nelson, *Phys. Rev. B* **22**, 2514 (1980).
- [31] L. Giomi, J. Toner, and N. Sarkar, *Phys. Rev. Lett.* **129**, 067801 (2022).
- [32] L. Giomi, J. Toner, and N. Sarkar, *Phys. Rev. E* **106**, 024701 (2022).
- [33] S. Hess, *Tensors for physics* (Springer, 2015).
- [34] M. Aubouy, Y. Jiang, J. A. Glazier, and F. Graner, *Granul. Matter* **5**, 67 (2003).
- [35] A. Brugués, E. Anon, V. Conte, J. H. Veldhuis, M. Gupta, J. Colombelli, J. J. Muñoz, G. W. Brodland, B. Ladoux, and X. Trepap, *Nat. Phys.* **8**, 683–690 (2014).
- [36] T. E. Angelini, E. Hannezo, X. Trepap, M. Marquez, J. J. Fredberg, and D. A. Weitz, *Proc. Natl. Acad. Sci. U.S.A.* **108**, 4714 (2011).
- [37] X. Trepap, M. R. Wasserman, T. E. Angelini, E. Millet, D. A. Weitz, J. P. Butler, and J. J. Fredberg, *Nat. Phys.* **5**, 426 (2009).
- [38] R. Voituriez, J. F. Joanny, and J. Prost, *Nat. Phys.* **70**, 404 (2005).
- [39] L. Giomi, *Phys. Rev. X* **5**, 031003 (2015).
- [40] C. Blanch-Mercader, V. Yashunsky, S. Garcia, G. Duclos, L. Giomi, and P. Silberzan, *Phys. Rev. Lett.* **120**, 208101 (2018).
- [41] Z. You, D. J. G. Pearce, A. Sengupta, and L. Giomi, *Phys. Rev. X* **8**, 031065 (2018).
- [42] S. B. Dierker and R. Pindak, *Phys. Rev. Lett.* **59**, 1002 (1987).
- [43] S. Sprunt and J. D. Litster, *Phys. Rev. Lett.* **59**, 2682 (1987).
- [44] R. Bruinsma and G. Aeppli, *Phys. Rev. Lett.* **48**, 1625 (1982).

- [45] J. V. Selinger and D. R. Nelson, *Phys. Rev. A* **39**, 3135 (1989).
- [46] J. V. Selinger, *J. Phys. II France* **11**, 1363 (1991).
- [47] V. Drouin-Touchette, P. P. Orth, P. Coleman, P. Chandra, and T. C. Lubensky, *Phys. Rev. X* **12**, 011043 (2022).
- [48] S. Ramaswamy, R. Aditi Simha, and J. Toner, *Europhys. Lett.* **62**, 196 (2003).
- [49] S. Shankar, S. Ramaswamy, and M. C. Marchetti, *Phys. Rev. E* **97**, 012707 (2018).
- [50] H. Chaté, *Annu. Rev. Condens. Matter Phys.* **11**, 189 (2020).
- [51] L. N. Carenza, G. Gonnella, A. Lamura, G. Negro, and A. Tiribocchi, *Eur. Phys. J. E* **42**, 81 (2019).
- [52] L. N. Carenza, L. Biferale, and G. Gonnella, *Eur. Phys. Lett.* **132**, 44003 (2020).
- [53] S. Tong, N. K. Singh, R. Sknepnek, and A. Košmrlj, *PLoS Comput. Biol.* **18**, e1010135 (2022).
- [54] M. J. Hertaeg, S. M. Fielding, and D. Bi, [arXiv:2211.15015](https://arxiv.org/abs/2211.15015) (2022), 10.48550/arXiv.2211.15015.
- [55] T. S. Majmudar and R. P. Behringer, *Nature* **435**, 1079 (2005).
- [56] G.-J. J. Gao, M. C. Holcomb, J. H. Thomas, and J. Blawdziewicz, *J. Phys.: Condens. Matter* **28**, 414021 (2016).
- [57] A. Amir and D. R. Nelson, *Proc. Natl. Acad. Sci* **109**, 9833 (2012).
- [58] J. T. Blankenship, S. T. Backovic, J. S. P. Sanny, O. Weitz, and J. A. Zallen, *Dev. Cell* **11**, 459 (2006).
- [59] M. Rauzi, *Phil. Trans. R. Soc. B* **375** (2020), 10.1098/rstb.2019.0552.
- [60] Y. Zhang and R. A. Weinberg, *Front. Med.* **12**, 361–373 (2018).

Hydrodynamics and multiscale order in confluent epithelia: Supplementary information

Josep-Maria Armengol-Collado,^{1,*} Livio N. Carenza,^{1,*} and Luca Giomi^{1,†}

¹*Instituut-Lorentz, Universiteit Leiden, P.O. Box 9506, 2300 RA Leiden, The Netherlands*

QUANTIFICATION OF p -ATIC ORDER IN EPITHELIAL LAYERS

Following [20], we use the *shape function* γ_p to quantify the amount of p -fold symmetry of an arbitrary cell. Denoting \mathbf{r}_v with $v = 1, 2 \dots V$, the positions of its vertices with respect to the cell's center of mass (CM), one has

$$\gamma_p = \frac{\sum_{v=1}^V |\mathbf{r}_v|^p e^{ip\phi_v}}{\sum_{v=1}^V |\mathbf{r}_v|^p}, \quad (\text{S1})$$

with $\phi_v = \text{Arg}(\mathbf{r}_v)$ the angle between \mathbf{r}_v and the x -axis of a Cartesian frame. A schematic representation of these elements in an arbitrary irregular polygon is shown in Fig. S1a. Unlike the complex function $\psi_p = e^{ip\vartheta}$, which has unit magnitude by construction, the magnitude $|\gamma_p|$ quantify the resemblance of a generic polygon with a *regular* p -sided polygon of the same size, while the phase $\vartheta = \text{Arg}(\gamma_p)/p$ marks the orientation of the polygon. For regular V -sided polygons, $|\gamma_p| = 1$ provided p is an integer multiple of V and $|\gamma_p| \approx 0$ otherwise. Furthermore, from γ_p one

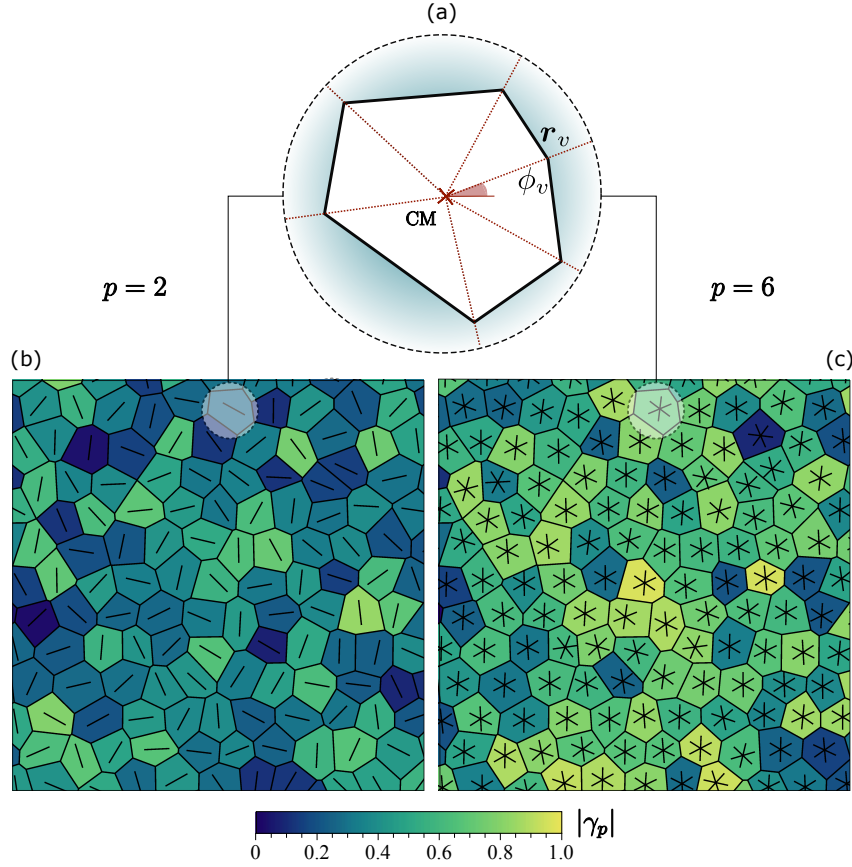


Fig. S1. (a) Irregular polygonal cell with a red cross marking its center of mass and \mathbf{r}_v and ϕ_v the radial vector and the angle to one of the six vertices respectively. (b) and (c) show the same tessellation of the plane with cells of different shapes and the shape analysis using the function in Eq. (S1) for the nematic ($p = 2$) and hexatic ($p = 6$) case. Rods and stars are oriented according to the phase of γ_p and the color corresponds to its magnitude.

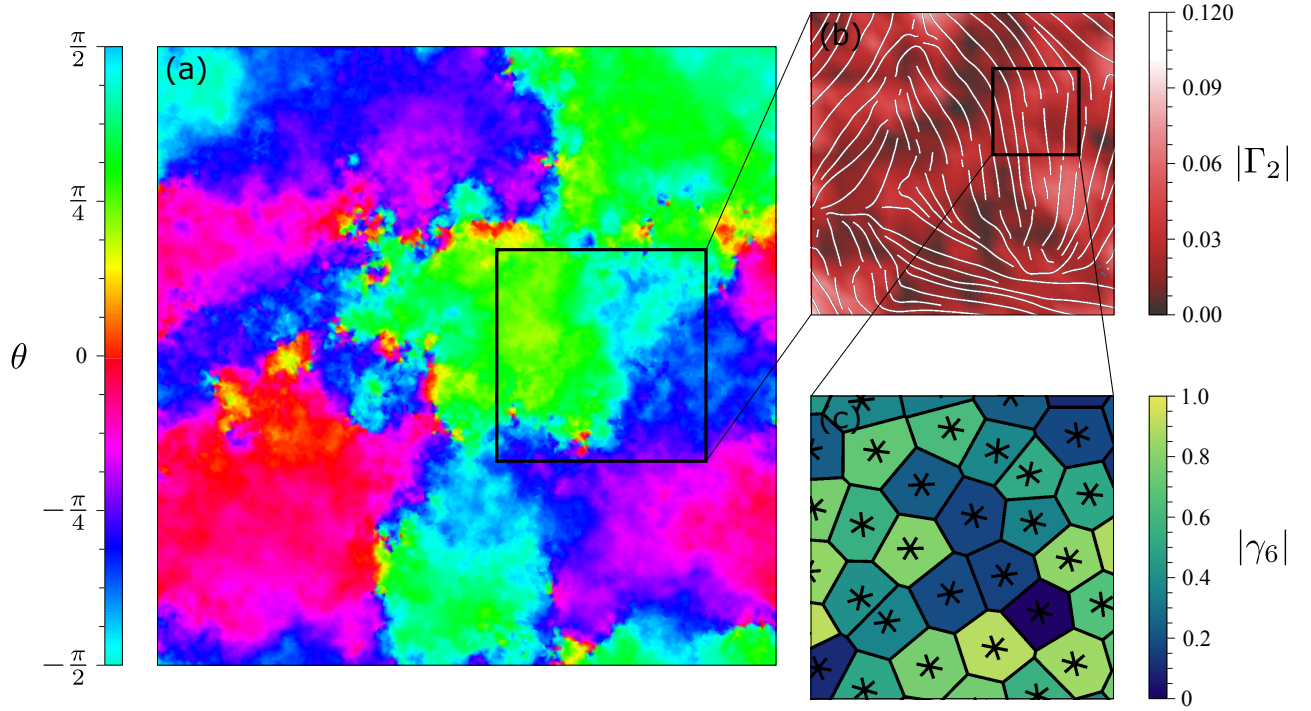


Fig. S2. (a) Coarse-grained nematic orientation θ obtained from averaging the local shape of cells over domains of size $30 \ell_{\text{cell}}$, with ℓ_{cell} the average size of individual cells. Regions with the same color represent domains of coherent nematic orientation. (b) Part of the system where we use Γ_2 to characterize the nematic phase. Solid lines represent the nematic director and the color indicates the magnitude of the nematic shape function. (c) Voronoi cell structure of a region where the nematic field is uniform. Polygons are colored according to $|\gamma_6|$ and the stars are oriented according to $\text{Arg}(\gamma_6)/6$.

can readily compute

$$\psi_p = \frac{\gamma_p}{|\gamma_p|}. \quad (\text{S2})$$

Figs. S1b and S1c shows examples of the functions γ_2 and γ_6 for a typical configuration of the SPV. We emphasize that γ_p , which, as show in Ref. [20], arises from a p -fold generalization of the classic shape tensor [34], is solely determined by the positions of the vertices of an individual polygon and, therefore, does not depend on the spatial organization of the neighbouring cells. As a consequence, this approach establishes an orientation purely based on cellular *shape*, thereby eliminating the arbitrariness involved with associating a network of bonds to a planar tessellation, where the latter is not inherent.

The shape function γ_p can then be coarse-grained at the length scale ℓ to construct the *shape parameter*:

$$\Gamma_p(\mathbf{r}) = \frac{1}{N_\ell} \sum_{c=1} \gamma_p(\mathbf{r}_c) \Theta(\ell - |\mathbf{r} - \mathbf{r}_c|), \quad (\text{S3})$$

where the \mathbf{r}_c is the position of the c -th cell, Θ is the Heaviside step function, such that $\Theta(x) = 1$ for $x > 0$ and 0 otherwise, and $N_\ell = \sum_c \Theta(\ell - |\mathbf{r} - \mathbf{r}_c|)$ is the number of cells within a distance ℓ from \mathbf{r}_c . As in the case of γ_p , the magnitude of Γ_p reflects the resemblance between a multicellular cluster and a regular p -sided polygon, while its phase marks the cluster's global orientation. The outcome of an application of this method to the Voronoi model is illustrated in Fig. S2 for $p = 2$. The different patches in panel (a) are regions with uniform $\theta = \text{Arg}(\Gamma_2)/2$, while in panel (b), there are plotted streamlines showing the orientation of the director $\mathbf{n} = \cos \theta \mathbf{e}_x + \sin \theta \mathbf{e}_y$.

PASSIVE STRESSES

As explained in the main text, the passive contribution to the stress tensor is given by $\boldsymbol{\sigma}^{(p)} = -P\mathbb{1} + \boldsymbol{\sigma}^{(e)} + \boldsymbol{\sigma}^{(r)} + \boldsymbol{\sigma}^{(v)}$, where, as demonstrated in [31, 32]

$$\sigma_{ij}^{(e)} = -L_p \partial_i \mathbf{Q}_p \odot \partial_j \mathbf{Q}_p, \quad (\text{S4a})$$

$$\sigma_{ij}^{(r)} = -\bar{\lambda}_p \mathbf{Q}_p \odot \mathbf{H}_p \delta_{ij} + (-1)^{p-1} \lambda_p \partial_{k_1 k_2 \dots k_{p-2}}^{p-2} H_{k_1 k_2 \dots ij} + \frac{p}{2} (Q_{k_1 k_2 \dots i} H_{k_1 k_2 \dots j} - H_{k_1 k_2 \dots i} Q_{k_1 k_2 \dots j}), \quad (\text{S4b})$$

$$\sigma_{ij}^{(v)} = 2\eta \llbracket u_{ij} \rrbracket + \zeta \text{tr}(\mathbf{u}) \delta_{ij}, \quad (\text{S4c})$$

where η and ζ are respectively the shear and bulk viscosity and the other material parameters are defined in the main text. Under the assumptions of uniform order parameter, i.e. $|\mathbf{Q}_p|^2 = |\Psi_p|^2/2 = \text{const}$, and taking $\lambda_p = 0$, Eq. (S4) reduces to the expression derived in [29, 30]. That is

$$\boldsymbol{\sigma}^{(e)} + \boldsymbol{\sigma}^{(r)} = -P\mathbb{1} + \frac{K_p}{2} \boldsymbol{\varepsilon} \nabla^2 \theta - K_p \nabla \theta \otimes \nabla \theta, \quad (\text{S5})$$

where the first term in Eq. (S4b) has incorporated into the pressure P and K_p denotes the orientational stiffness of the p -atic phase, related to the order parameter stiffness by

$$K_p = \frac{p^2 |\Psi_p|^2}{2} L_p \quad (\text{S6})$$

and $\boldsymbol{\varepsilon}$ is the two-dimensional antisymmetric tensor, with $\varepsilon_{xy} = -\varepsilon_{yx} = 1$ and $\varepsilon_{xx} = \varepsilon_{yy} = 0$.

LINEAR FLUCTUATING HYDRODYNAMICS

To compute the structure factor, we follow [48] and augment Eqs. (2b) and (2c) with short-ranged correlated noise field. Then calling ϑ and φ the nematic and hexatic *fluctuating* orientation fields and linearizing the hydrodynamic equations about the homogeneous and stationary solutions, $\vartheta = \varphi = 0$ and $\mathbf{v} = \mathbf{0}$, gives

$$\partial_t \delta \rho = -\rho_0 \nabla \cdot \delta \mathbf{v}, \quad (\text{S7a})$$

$$\partial_t \delta \vartheta = \mathcal{D}_2 \nabla^2 \delta \vartheta + \frac{1}{2} \mathbf{e}_z \cdot (\nabla \times \delta \mathbf{v}) + \frac{9}{4} \chi_2 (\delta \vartheta - \delta \varphi) + \xi^{(\vartheta)}, \quad (\text{S7b})$$

$$\partial_t \delta \varphi = \mathcal{D}_6 \nabla^2 \delta \varphi + \frac{1}{2} \mathbf{e}_z \cdot (\nabla \times \delta \mathbf{v}) + \frac{1}{4} \chi_6 (\delta \varphi - \delta \vartheta) + \xi^{(\varphi)}, \quad (\text{S7c})$$

where $\delta \vartheta$, $\delta \varphi$ and $\delta \mathbf{v}$ indicate a small departure from the homogeneous and stationary configurations of the fields ϑ , φ and \mathbf{v} , $\mathcal{D}_p = \Gamma_p L_p$, $\chi_p = \Gamma_p \chi_{2,6}$, and $\xi^{(\vartheta)}$ and $\xi^{(\varphi)}$ are short-ranged correlated noise fields: i.e.

$$\langle \xi^{(\alpha)}(\mathbf{r}, t) \xi^{(\beta)}(\mathbf{r}', t') \rangle = 2 \left(\Xi^{(\vartheta)} \delta_{\alpha\vartheta} \delta_{\beta\vartheta} + \Xi^{(\varphi)} \delta_{\alpha\varphi} \delta_{\beta\varphi} \right) \delta(\mathbf{r} - \mathbf{r}') \delta(t - t'). \quad (\text{S8})$$

The velocity field $\delta \mathbf{v}$, on the other hand, is found from the Stokes limit of Eq. (2b) in the main text, which, at the linear order in all fluctuating fields, takes the form

$$\eta \nabla^2 \delta \mathbf{v} + \zeta \nabla (\nabla \cdot \delta \mathbf{v}) - \varsigma \delta \mathbf{v} + \mathbf{f}^{(p)} + \mathbf{f}^{(a)} + \boldsymbol{\xi}^{(v)} = \mathbf{0}. \quad (\text{S9})$$

where $\mathbf{f}^{(p)} = \nabla \cdot \boldsymbol{\sigma}^{(p)}$ and $\mathbf{f}^{(a)} = \nabla \cdot \boldsymbol{\sigma}^{(a)}$ are the body forces resulting from the passive and active stresses respectively. The quantity $\boldsymbol{\xi}^{(v)}$ is a translational noise field. In the absence of external stimuli, it is reasonable to assume that global momentum is neither created nor dissipated by translational fluctuations, but only redistributed across the cell layer. Thus $\boldsymbol{\xi}^{(v)}$ is either conservative or null, from which

$$\langle \xi_i^{(v)}(\mathbf{r}, t) \xi_j^{(v)}(\mathbf{r}', t') \rangle = 2 \Xi^{(v)} \delta_{ij} (-\nabla^2) \delta(\mathbf{r} - \mathbf{r}') \delta(t - t'), \quad (\text{S10})$$

with $\{i, j\} \in \{x, y\}$ and the case of noiseless translational dynamics, corresponding to Fig. (3) in the main text, is recovered in the limit $\Xi^{(v)} \rightarrow 0$. The pressure P , in turn, can be related to the density by a linear equation of state of the form

$$P = c_s^2 \rho, \quad (\text{S11})$$

with c_s the speed of sound. Together with the expression for the active stress given in Eq. (3) of the main text, this gives

$$\mathbf{f}^{(p)} = \left(-c_s^2 \partial_x \delta \rho + \frac{K_2}{2} \partial_y \nabla^2 \delta \vartheta + \frac{K_6}{2} \partial_y \nabla^2 \delta \varphi \right) \mathbf{e}_x - \left(c_s^2 \partial_y \delta \rho + \frac{K_2}{2} \partial_x \nabla^2 \delta \vartheta + \frac{K_6}{2} \partial_x \nabla^2 \delta \varphi \right) \mathbf{e}_y, \quad (\text{S12a})$$

$$\mathbf{f}^{(a)} = \left[\alpha_2 \partial_y \delta \vartheta + \frac{3}{2} \alpha_6 \left(\partial_y^4 - 5 \partial_x^2 \partial_y^2 + \frac{5}{2} \partial_x^4 \right) \partial_y \delta \varphi \right] \mathbf{e}_x + \left[\alpha_2 \partial_x \delta \vartheta + \frac{3}{2} \alpha_6 \left(\partial_x^4 - 5 \partial_x^2 \partial_y^2 + \frac{5}{2} \partial_y^4 \right) \partial_x \delta \varphi \right] \mathbf{e}_y. \quad (\text{S12b})$$

Now, in Fourier space Eq. (S9) can be cast in the form of the following linear algebraic equation

$$[(\eta|\mathbf{q}|^2 + \varsigma) \mathbb{1} + \zeta \mathbf{q} \otimes \mathbf{q}] \cdot \delta \hat{\mathbf{v}} = \hat{\mathbf{f}}^{(p)} + \hat{\mathbf{f}}^{(a)} + \hat{\boldsymbol{\xi}}^{(v)}, \quad (\text{S13})$$

where the hat denotes Fourier transformation. Next, using

$$[(\eta|\mathbf{q}|^2 + \varsigma) \mathbb{1} + \zeta \mathbf{q} \otimes \mathbf{q}]^{-1} = \frac{[(\eta + \zeta)|\mathbf{q}|^2 + \varsigma] \mathbb{1} - \zeta \mathbf{q} \otimes \mathbf{q}}{(\eta|\mathbf{q}|^2 + \varsigma)[(\eta + \zeta)|\mathbf{q}|^2 + \varsigma]}, \quad (\text{S14})$$

and solving Eq. (S13) and incorporating the resulting velocity field in Eqs. (S7) gives, after several algebraic manipulation

$$-i\omega \begin{bmatrix} \delta \hat{\rho} \\ \delta \hat{\vartheta} \\ \delta \hat{\varphi} \end{bmatrix} = \hat{\mathbf{M}} \cdot \begin{bmatrix} \delta \hat{\rho} \\ \delta \hat{\vartheta} \\ \delta \hat{\varphi} \end{bmatrix} + \begin{bmatrix} \hat{\eta}^{(\rho)} \\ \hat{\eta}^{(\vartheta)} \\ \hat{\eta}^{(\varphi)} \end{bmatrix}, \quad (\text{S15})$$

where the matrix $\hat{\mathbf{M}}$ is given by

$$\hat{\mathbf{M}} = \begin{bmatrix} -\frac{\rho_0 c_s^2 |\mathbf{q}|^2}{(\eta + \zeta)|\mathbf{q}|^2 + \varsigma} & \frac{2\rho_0 \alpha_2 q_x q_y}{(\eta + \zeta)|\mathbf{q}|^2 + \varsigma} & \frac{3\rho_0 \alpha_6 (3q_x^5 q_y - 10q_x^3 q_y^3 + 3q_x q_y^5)}{2[(\eta + \zeta)|\mathbf{q}|^2 + \varsigma]} \\ 0 & -\mathcal{D}_2 |\mathbf{q}|^2 - \frac{K_2 |\mathbf{q}|^4}{4(\eta|\mathbf{q}|^2 + \varsigma)} + \frac{9}{4} \chi_2 - \frac{\alpha_2 (q_x^2 - q_y^2)}{2(\eta|\mathbf{q}|^2 + \varsigma)} & -\frac{K_6 |\mathbf{q}|^4}{4(\eta|\mathbf{q}|^2 + \varsigma)} - \frac{9}{4} \chi_2 - \frac{3\alpha_6 (q_x^6 - 15q_x^4 q_y^2 + 15q_x^2 q_y^4 - q_y^6)}{8(\eta|\mathbf{q}|^2 + \varsigma)} \\ 0 & -\frac{K_2 |\mathbf{q}|^4}{4(\eta|\mathbf{q}|^2 + \varsigma)} - \frac{1}{4} \chi_6 - \frac{\alpha_2 (q_x^2 - q_y^2)}{2(\eta|\mathbf{q}|^2 + \varsigma)} & -\mathcal{D}_6 |\mathbf{q}|^2 - \frac{K_6 |\mathbf{q}|^4}{4(\eta|\mathbf{q}|^2 + \varsigma)} + \frac{1}{4} \chi_6 - \frac{3\alpha_6 (q_x^6 - 15q_x^4 q_y^2 + 15q_x^2 q_y^4 - q_y^6)}{8(\eta|\mathbf{q}|^2 + \varsigma)} \end{bmatrix},$$

and the functions $\hat{\eta}^{(\alpha)}$, with $\alpha \in \{\rho, \vartheta, \varphi\}$, are effective noise fields whose correlation functions are given by

$$\langle \hat{\eta}^{(\alpha)}(\mathbf{q}, \omega) \hat{\eta}^{(\beta)}(\mathbf{q}', \omega') \rangle = (2\pi)^3 2\hat{H}^{(\alpha)}(\mathbf{q}) \delta_{\alpha\beta} \delta(\mathbf{q} + \mathbf{q}') \delta(\omega + \omega'), \quad (\text{S16})$$

where the functions $\hat{H}^{(\alpha)} = \hat{H}^{(\alpha)}(\mathbf{q})$ are given by

$$\hat{H}^{(\rho)} = \frac{\rho_0^2 |\mathbf{q}|^4}{[(\eta + \zeta)|\mathbf{q}|^2 + \varsigma]^2} \Xi^{(v)}, \quad (\text{S17})$$

$$\hat{H}^{(\alpha)} = \Xi^{(\vartheta)} \delta_{\alpha\vartheta} + \Xi^{(\varphi)} \delta_{\alpha\varphi} + \frac{|\mathbf{q}|^4}{4(\eta|\mathbf{q}|^2 + \varsigma)^2} \Xi^{(v)}. \quad (\text{S18})$$

Notice that, while hydrodynamic flow has the effect of coloring the orientational noise embodied in the stochastic fields $\xi^{(\vartheta)}$ and $\xi^{(\varphi)}$, via the vorticity field on the right-hand side of Eqs. (S7b) and (S7c), this effect disappears at the small (i.e. $|\mathbf{q}| \rightarrow \infty$) and large (i.e. $|\mathbf{q}| \rightarrow 0$) scale, as long as *both* viscous and frictional dissipation are present.

STRUCTURE FACTOR

The static structure factor can be expressed in integral form as

$$S(\mathbf{q}) = \int_{-\infty}^{\infty} \frac{d\omega}{2\pi} S(\mathbf{q}, \omega). \quad (\text{S19})$$

where the dynamic structure factor $S(\mathbf{q}, \omega)$, can be calculated from the correlation function

$$\langle \delta \hat{\rho}(\mathbf{q}, \omega) \delta \hat{\rho}(\mathbf{q}', \omega') \rangle = (2\pi)^3 S(\mathbf{q}, \omega) \delta(\mathbf{q} + \mathbf{q}') \delta(\omega + \omega'). \quad (\text{S20})$$

To compute the left-hand side of Eq. (S20) one can solve Eq. (S15) with respect to $\delta\hat{\rho}$, $\delta\hat{\vartheta}$ and $\delta\hat{\varphi}$. This gives

$$\delta\hat{\rho} = \frac{i\hat{\eta}^{(\rho)}}{\omega - i\hat{M}_{\rho\rho}} - \frac{\hat{\eta}^{(\vartheta)} \left[\hat{M}_{\rho\vartheta} (\omega - i\hat{M}_{\varphi\varphi}) + i\hat{M}_{\rho\varphi}\hat{M}_{\varphi\vartheta} \right] + \hat{\eta}^{(\varphi)} \left[\hat{M}_{\rho\varphi} (\omega - i\hat{M}_{\vartheta\vartheta}) + i\hat{M}_{\rho\vartheta}\hat{M}_{\varphi\varphi} \right]}{(\omega - i\hat{M}_{\rho\rho}) \left[\omega^2 - i\omega(\hat{M}_{\vartheta\vartheta} + \hat{M}_{\varphi\varphi}) - \hat{M}_{\vartheta\vartheta}\hat{M}_{\varphi\varphi} + \hat{M}_{\vartheta\varphi}\hat{M}_{\varphi\vartheta} \right]}, \quad (\text{S21a})$$

$$\delta\hat{\vartheta} = \frac{\hat{\eta}^{(\vartheta)}(i\omega + \hat{M}_{\varphi\varphi}) - \hat{\eta}^{(\varphi)}\hat{M}_{\vartheta\varphi}}{\left[\omega^2 - i\omega(\hat{M}_{\vartheta\vartheta} + \hat{M}_{\varphi\varphi}) - \hat{M}_{\vartheta\vartheta}\hat{M}_{\varphi\varphi} + \hat{M}_{\vartheta\varphi}\hat{M}_{\varphi\vartheta} \right]}, \quad (\text{S21b})$$

$$\delta\hat{\varphi} = \frac{\hat{\eta}^{(\varphi)}(i\omega + \hat{M}_{\vartheta\vartheta}) - \hat{\eta}^{(\vartheta)}\hat{M}_{\varphi\vartheta}}{\left[\omega^2 - i\omega(\hat{M}_{\vartheta\vartheta} + \hat{M}_{\varphi\varphi}) - \hat{M}_{\vartheta\vartheta}\hat{M}_{\varphi\varphi} + \hat{M}_{\vartheta\varphi}\hat{M}_{\varphi\vartheta} \right]}. \quad (\text{S21c})$$

The static structure factor can then be expressed as

$$S = S^{(\rho)} + S^{(\vartheta)} + S^{(\varphi)}. \quad (\text{S22})$$

The first term on the right-hand side can be readily calculated in the form

$$S^{(\rho)} = \int_{-\infty}^{\infty} \frac{d\omega}{\pi} \frac{\hat{H}^{(\rho)}}{\hat{M}_{\rho\rho}^2 + \omega^2} = \frac{\hat{H}^{(\rho)}}{|\hat{M}_{\rho\rho}|} = \frac{\rho_0 |\mathbf{q}|^2 \Xi^{(v)}}{c_s^2 [(\eta + \zeta) |\mathbf{q}|^2 + \varsigma]}, \quad (\text{S23})$$

indicating that, if driven solely by pressure fluctuations, the system would relax toward a structureless homogeneous state with $S \rightarrow \rho_0 \Xi^{(\rho)} / (\zeta c_s^2)$ when $|\mathbf{q}| \rightarrow 0$. The effect of the active currents is instead accounted for by the second and third term on the right-hand side of Eq. (S22), which can be cast in the general form

$$S^{(\alpha)} = H^{(\alpha)} \int_{-\infty}^{\infty} \frac{d\omega}{\pi} \frac{g^{(\alpha)}(\omega)}{|h(\omega)|^2}, \quad \alpha = \{\vartheta, \varphi\}, \quad (\text{S24})$$

where

$$g^{(\vartheta)}(\omega) = (\hat{M}_{\rho\vartheta}\omega)^2 + (\hat{M}_{\rho\varphi}\hat{M}_{\varphi\vartheta} - \hat{M}_{\rho\vartheta}\hat{M}_{\varphi\varphi})^2, \quad (\text{S25a})$$

$$g^{(\varphi)}(\omega) = (\hat{M}_{\rho\varphi}\omega)^2 + (\hat{M}_{\rho\vartheta}\hat{M}_{\vartheta\varphi} - \hat{M}_{\rho\varphi}\hat{M}_{\vartheta\vartheta})^2, \quad (\text{S25b})$$

$$h(\omega) = (\omega - i\hat{M}_{\rho\rho}) \left[\omega^2 - i\omega(\hat{M}_{\vartheta\vartheta} + \hat{M}_{\varphi\varphi}) - \hat{M}_{\vartheta\vartheta}\hat{M}_{\varphi\varphi} + \hat{M}_{\vartheta\varphi}\hat{M}_{\varphi\vartheta} \right]. \quad (\text{S25c})$$

The integral over ω can be derived using the residue theorem upon computing the roots of the complex third-order polynomial h . To make progress, we express

$$|h(\omega)|^2 = (\omega^2 + \omega_1^2)(\omega^2 + \omega_2^2)(\omega^2 + \omega_3^2), \quad (\text{S26})$$

where ω_1 , ω_2 and ω_3 are given by

$$\omega_1 = \hat{M}_{\rho\rho}, \quad (\text{S27a})$$

$$\omega_2 = \frac{1}{2} \left(\hat{M}_{\vartheta\vartheta} + \hat{M}_{\varphi\varphi} - \sqrt{(\hat{M}_{\vartheta\vartheta} - \hat{M}_{\varphi\varphi})^2 + 4\hat{M}_{\vartheta\varphi}\hat{M}_{\varphi\vartheta}} \right), \quad (\text{S27b})$$

$$\omega_3 = \frac{1}{2} \left(\hat{M}_{\vartheta\vartheta} + \hat{M}_{\varphi\varphi} + \sqrt{(\hat{M}_{\vartheta\vartheta} - \hat{M}_{\varphi\varphi})^2 + 4\hat{M}_{\vartheta\varphi}\hat{M}_{\varphi\vartheta}} \right). \quad (\text{S27c})$$

The integrand on the right-hand side of Eq. (S24) has, therefore, three pairs of purely imaginary poles: i.e. $\pm i|\omega_1|$, $\pm i|\omega_2|$ and $\pm i|\omega_3|$. Next, turning the integration range to an infinite semicircular contour on the complex upper half-plane and summing the associated residues gives, after lengthy algebraic manipulations

$$S^{(\vartheta)} = \frac{H^{(\vartheta)} \left[\Omega_1 \hat{M}_{\rho\vartheta}^2 + \Omega_2 (\hat{M}_{\rho\varphi}\hat{M}_{\varphi\vartheta} - \hat{M}_{\rho\vartheta}\hat{M}_{\varphi\varphi})^2 \right]}{\Omega_1 \Omega_2 \Omega_3 - \Omega_1^2}, \quad (\text{S28a})$$

$$S^{(\varphi)} = \frac{H^{(\varphi)} \left[\Omega_1 \hat{M}_{\rho\varphi}^2 + \Omega_2 (\hat{M}_{\rho\vartheta}\hat{M}_{\vartheta\varphi} - \hat{M}_{\rho\varphi}\hat{M}_{\vartheta\vartheta})^2 \right]}{\Omega_1 \Omega_2 \Omega_3 - \Omega_1^2}, \quad (\text{S28b})$$

where we have set

$$\Omega_1 = |\omega_1||\omega_2||\omega_3|, \quad (\text{S29a})$$

$$\Omega_2 = |\omega_1| + |\omega_2| + |\omega_3|, \quad (\text{S29b})$$

$$\Omega_3 = |\omega_1||\omega_2| + |\omega_1||\omega_3| + |\omega_2||\omega_3|. \quad (\text{S29c})$$

Now, although the individual elements of the matrix $\hat{\mathbf{M}}$ depend on the individual components of the wave vector – i.e. q_x and q_y – this is an artefact of linearizing the hydrodynamic equations about a specific orientation (i.e. $\vartheta = \varphi = 0$ in this case). Because of the lack of long-ranged order and of specific directions that could affect the spectrum of density fluctuations, the latter is expected to be isotropic, thus $S = S(|\mathbf{q}|)$. To remove the fictitious angular dependence, one can either linearize Eqs. (2) about a generic pair of angles, ϑ_0 and φ_0 , and then use these to calculate a circular average – i.e. $S(|\mathbf{q}|) = 1/(2\pi)^2 \int d\vartheta_0 d\varphi_0 S(\mathbf{q})$ – or, more simply, by orienting $\hat{\mathbf{q}}$ so to cancel the directional dependence. Thus, taking $q_x = q_y = |\mathbf{q}|/\sqrt{2}$ gives a simpler expression of the matrix $\hat{\mathbf{M}}$. That is

$$\hat{\mathbf{M}} = \begin{bmatrix} -\frac{\rho_0 c_s^2 |\mathbf{q}|^2}{(\eta+\zeta)|\mathbf{q}|^2+\varsigma} & \frac{\rho_0 \alpha_2 |\mathbf{q}|^2}{(\eta+\zeta)|\mathbf{q}|^2+\varsigma} & -\frac{3\rho_0 \alpha_6 |\mathbf{q}|^6}{4[(\eta+\zeta)|\mathbf{q}|^2+\varsigma]} \\ 0 & -\mathcal{D}_2 |\mathbf{q}|^2 - \frac{K_2 |\mathbf{q}|^4}{4(\eta|\mathbf{q}|^2+\varsigma)} + \frac{9}{4}\chi_2 & -\frac{K_6 |\mathbf{q}|^4}{4(\eta|\mathbf{q}|^2+\varsigma)} - \frac{9}{4}\chi_2 \\ 0 & -\frac{K_2 |\mathbf{q}|^4}{4(\eta|\mathbf{q}|^2+\varsigma)} - \frac{1}{4}\chi_6 & -\mathcal{D}_6 |\mathbf{q}|^2 - \frac{K_6 |\mathbf{q}|^4}{4(\eta|\mathbf{q}|^2+\varsigma)} + \frac{1}{4}\chi_6 \end{bmatrix}. \quad (\text{S30})$$

Using the elements of this matrix in combination with Eqs. (S22), (S24), (S27) and (S29) yields the curves plotted in Fig. (3). Finally, asymptotically expanding Eq. (S22) allows one, after lengthy algebraic manipulations, to calculate the coefficients s_{-2} and s_4 in Eq. (8). That is

$$s_{-2} = \frac{\rho_0 \alpha_2^2 [(9\chi_2)^2 \Xi_\varphi + \chi_6^2 \Xi_\vartheta]}{c_s^2 (9\chi_2 \mathcal{D}_6 + \chi_6 \mathcal{D}_2) [\rho_0 c_s^2 (9\chi_2 + \chi_6) + \varsigma (9\chi_2 \mathcal{D}_6 + \chi_6 \mathcal{D}_2)]}, \quad (\text{S31a})$$

$$s_4 = \frac{72\rho_0 \alpha_6^2 [(K_2^2 + 8\eta \mathcal{D}_2 K_2 + 8\eta^2 \mathcal{D}_2^2) \Xi^{(\nu)} + K_2^2 \Xi_\vartheta + 2\eta^2 (K_2 + 4\eta \mathcal{D}_2)^2 \Xi_\varphi]}{c_s^2 (\eta + \zeta) [K_2 + K_6 + 4\eta (\mathcal{D}_2 + \mathcal{D}_6)]^4}. \quad (\text{S31b})$$

Notice that, while both orientational and translation noise affect the amplitude of density fluctuations at small length scales, where $S(|\mathbf{q}|) \sim s_4 |\mathbf{q}|^4$, translational noise becomes unimportant at the large scale, where $S(|\mathbf{q}|) \sim s_{-2}/|\mathbf{q}|^2$. Furthermore, as long as viscous dissipation is at play, switching off translational noise (i.e. $\Xi^{(\nu)} \rightarrow 0$) does not alter the scaling behavior of the structure factor at neither range of length scales. Taking the dry limit (i.e. $\eta \rightarrow 0$ and $\zeta \rightarrow 0$) leaves the large scale behavior unaltered, but does affect the scaling of density fluctuations at short length scales, where translational fluctuations are most prominent. Specifically, $S(|\mathbf{q}|) \sim s_6 |\mathbf{q}|^6$ in the case of purely rotational noise and $S(|\mathbf{q}|) \sim s_{10} |\mathbf{q}|^{10}$ in the presence of rototranslational noise. The coefficients s_6 and s_{10} can be computed as in the viscous case, to give

$$s_6 = \left(\frac{3}{2}\right)^2 \frac{\rho_0^2 \alpha_6^2 \Xi^{(\varphi)}}{\varsigma^2 (\mathcal{D}_2 + \mathcal{D}_6)^3}, \quad (\text{S32a})$$

$$s_{10} = \left(\frac{3}{4}\right)^2 \frac{\rho_0^2 \alpha_6^2 \Xi^{(\varphi)}}{\varsigma^4 (\mathcal{D}_2 + \mathcal{D}_6)^3}. \quad (\text{S32b})$$

NUMERICAL METHODS

The Voronoi model

In the self-propelled Voronoi model (SVM) [8] a confluent cell layer is approximated as a Voronoi tessellation of the plane. Each cell is characterized by the position \mathbf{r}_c of its center, with $c = 1, 2, \dots, N$, and a velocity $\mathbf{v}_c = v_0 (\cos \theta_c \mathbf{e}_x + \sin \theta_c \mathbf{e}_y)$, with v_0 a constant speed and θ_c an orientation. We stress that, in general, the center of a Voronoi polygon does not correspond to the polygon's centroid (i.e. center of mass). The dynamics of these variables is governed by the following set of overdamped Langevin equations, expressing the interplay between cells' autonomous

motion and the remodelling events that underlie the tissue's collective dynamics. That is:

$$\frac{d\mathbf{r}_c}{dt} = \mathbf{v}_c - \mu \nabla_{\mathbf{r}_c} E, \quad (\text{S33a})$$

$$\frac{d\theta_c}{dt} = \eta_c, \quad (\text{S33b})$$

where μ is the mobility coefficient and $E = E(\mathbf{r}_1, \mathbf{r}_2 \dots \mathbf{r}_N)$ is an energy function involving exclusively geometrical quantities, such as the area A_c and the perimeter P_c of each cell: i.e.

$$E = \sum_c \left[K_A (A_c - A_0)^2 + K_P (P_c - P_0)^2 \right], \quad (\text{S34})$$

with K_A , K_P , A_0 and P_0 constants. The first term in Eq. (S34) embodies a combination of cells' volumetric incompressibility and monolayer resistance to thickness fluctuations. The second term results from the cytoskeletal contractility (quadratic in P_c) and the effective interfacial tension caused by the cell-cell adhesion and the cortical tension (both linear in P_c) [6]. The constants A_0 and P_0 represent, respectively, the preferred area and perimeter of each cell. The quantity η_c , on the other hand, is a random number with zero mean and correlation function

$$\langle \eta_c(t) \eta_{c'}(t') \rangle = 2\mathcal{D}_r \delta_{cc'} \delta(t - t'), \quad (\text{S35})$$

with \mathcal{D}_r a rotational diffusion coefficient. To make progress, we next introduce the following dimensionless numbers: the shape index $p_0 = P_0/\sqrt{A_0}$, which accounts for the spontaneous degree of acircularity of individual cells [8], and the Péclet number $\text{Pe} = v_0/(\mathcal{D}_r \sqrt{A_0})$, which quantifies the persistence of directed cellular motion in front of their diffusivity.

To obtain the plots in Fig. (3), we numerically integrate Eqs. (S33) in a domain of size L_g with periodic boundary conditions. At $t = 0$, the centroids \mathbf{r}_c are placed in a slightly perturbed hexagonal grid with a random initial velocity. After reaching the non-equilibrium steady state, we perform statistical averages of relevant observables. In our numerical simulations, we set $p_0 = 3.85$, $\mu K_A A_0 / \mathcal{D}_r = 1$, $\mu K_P / \mathcal{D}_r = 1$, and $\mathcal{D}_r \Delta t = 5 \times 10^{-3}$, where Δt is the time-step used for the integration, and the average density of particles $NA_0/L_g^2 = 1$. We vary the Péclet number in the range $0.1 \leq \text{Pe} \leq 2.0$. The results presented in Results are robust to the variation of the system size, as no qualitative difference was observed upon varying the domain size in the range $30 \leq L_g \leq 200$ at constant density. The density structure factor (light green circles) in Fig. (3) a was obtained, in particular, with $\text{Pe} = 1.5$.

The Multiphase field model

The multiphase field (MPF) model is a continuous model where each cell is described by a concentration field $\varphi_c = \varphi_c(\mathbf{r})$ with $c = 1, 2 \dots N$ and N the total number of cells. This model has been used to study the dynamics of confluent cell monolayers [11] and the mechanics of cell extrusion [12]. Equilibrium configurations are obtained upon relaxing the free energy $\mathcal{F} = \int dA f$, where the free energy density f is given by

$$f = \frac{\alpha}{4} \sum_c \varphi_c^2 (\varphi_c - \varphi_0)^2 + \frac{k_\varphi}{2} \sum_c (\nabla \varphi_c)^2 + \epsilon \sum_{c < c'} \varphi_c^2 \varphi_{c'}^2 + \sum_c \lambda \left(1 - \frac{1}{\pi \phi_0^2 R_\varphi^2} \int dA \varphi_c^2 \right)^2. \quad (\text{S36})$$

Here α and k_ϕ are material parameters which can be used to tune the surface tension $\gamma = (8k_\varphi \alpha / 9)^{1/2}$ and the interfacial thickness $\xi = (2k_\varphi / \alpha)^{1/2}$ of isolated cells and thermodynamically favor spherical cell shapes. The constant ϵ captures the repulsion between cells. The concentration field is large (i.e. $\varphi_c \simeq \phi_0$) inside the cells and zero outside. The contribution proportional to λ in the free energy enforces cell incompressibility whose nominal radius is given by R_φ . The relaxational dynamics of the field φ_c is governed by the Allen-Cahn equation

$$\partial_t \varphi_c + \mathbf{v}_c \cdot \nabla \varphi_c = -M \frac{\delta \mathcal{F}}{\delta \varphi_c}, \quad (\text{S37})$$

where \mathbf{v}_c has the same meaning as in the SPV model described in the previous section and its dynamics is also governed by Eq. (S33b). The constant M in Eq. (S37) is the mobility measuring the relevance of thermodynamic relaxation with respect to non-equilibrium cell migration. The dimensionless parameters of the model are the Péclet number $\text{Pe} = v_0/(2\mathcal{D}_r R_\varphi)$ and the cell deformability $d = \epsilon/\alpha$.

The system of partial differential equations, Eq. (S37), is solved with a finite-difference approach through a predictor-corrector finite difference Euler scheme implementing second order stencil for space derivatives [51]. The C-code implemented for numerical integration is parallelized by means of MPI. We consider systems of $N = 361$ cells in a square domain of $L_g = 380$ grid points. Model parameters in simulation units are as follows: $R_\phi = 11$, $\varphi_0 = 2.0$, $M\alpha = 0.006$, $M\kappa_\varphi = 0.006$, $M\epsilon = 0.01$, $M\lambda = 600$, $M\gamma = 0.008$, $D_r\Delta t = 10^{-4}$, being Δt the time-step used to integrate Eq. (S37). We vary the speed of self-propulsion in the range $0.0 \leq v_0 \leq 0.005$. In terms of dimensionless parameters this corresponds to having $d = 1.66$ and Pe ranging between 0 and 2.30. The timescale of cell motility with respect to the timescale of elastic relaxation driven by surface tension $v_0/(M\gamma)$ ranges between 0 and 0.625. Moreover, the nominal packing fraction is $N(\pi R_\phi^2)/L_g^2 = 0.95$, while the ratio between the interface thickness and the nominal radius $\xi/R_\phi = 0.12$. The density structure factor (dark green triangles) in Fig. (3)a was obtained with $Pe = 1.38$.

NUMERICAL METHOD FOR INTEGRATION OF THE HYDRODYNAMIC EQUATIONS

Eqs. [2] have been integrated by means of a hybrid Lattice Boltzmann (LB) method, in which Eq. (2b) is solved through a predictor-corrector LB algorithm and the remaining equations via a predictor-corrector finite-difference Euler approach, with a first-order upwind scheme and second-order accurate stencils for the computation of spacial derivatives [51]. The code has been parallelized by means of Message Passage Interface (MPI), by dividing the computational domain in slices and by implementing the ghost-cell method to compute derivatives on the boundary of the computational subdomains. Runs have been performed using 64 CPUs in two-dimensional geometries, on a computational box of size 256^2 and 512^2 , for at least 1.5×10^7 lattice Boltzmann iterations (corresponding to ~ 21 days and ~ 84 days of CPU-time, respectively for the smaller and larger computational boxes). Periodic boundary conditions have been imposed. The director fields (for both $p = 2$ and $p = 6$) have been randomly initialized. The initial density field is assumed to be uniform with $\rho = 2.0$ everywhere. The model parameters in simulation units are as follows: $\eta = \zeta = 1.66$, $\lambda_2 = \lambda_6 = 1.1$, $\nu_2 = \nu_6 = 0.0$, $\Gamma_2 = 0.4$, $A_2 = -B_2 = -0.04$, $L_2 = 0.04$, $\Gamma_6 = 0.4$, $A_6 = -B_6 = -0.004$, $L_6 = 0.004$, $\kappa_{2,6} = \xi_{2,6} = -0.004$. Nematic activity α_2 has been varied in the range $-0.02 \leq \alpha_2 \leq -0.0005$ and hexatic activity α_6 in the range $-0.050 \leq \alpha_6 \leq 0.050$. We set the active parameters β_2 and $\beta_6 = 0$. The density structure factor (continuous black line) in Fig. (3) was obtained with $\alpha_2 = -2 \times 10^{-3}$ and $\alpha_6 = 2 \times 10^{-2}$.

The coherence length of the nematic and hexatic liquid crystal can be expressed as the $(L_p/A_p)^{1/2} = \Delta x_{LB}$ for both $p = 2, 6$, where Δx_{LB} is the grid spacing of the lattice Boltzmann algorithm. The active lengthscale as defined in the main text is given for the active nematics as ℓ_2 and ranges between $10\Delta x_{LB}$ for $\alpha_2 = -0.0005$ and $1.5\Delta x_{LB}$ for $\alpha_2 = -0.02$. Conversely, for hexatics ℓ_6 and ranges up to $3.5\Delta x_{LB}$ for $|\alpha_6| = 0.05$. To compare the results of the hydrodynamics simulations with the discrete models in Fig. (3a), we choose $2\Delta x_{LB} = \sqrt{A_0}$ and $2\Delta x_{LB} = R_\phi\Delta x_{MP}$, with Δx_{MP} the grid spacing used to integrate Eq. (S37).

COMPARISON WITH PASSIVE LIQUID CRYSTALS WITH COUPLED ORDER PARAMETERS

In this section we show how multiscale *hexanematic* order differs from previously reported examples of liquid crystal order with coupled order parameters [44, 45, 46]. To quantify the interplay between nematic and hexatic order, here we focus on the function $C_{26}(\mathbf{r})$ given in Eq. [9], reflecting the amount of cross-correlation in their fluctuations. Here $\psi_2 = e^{2i\vartheta}$ and $\psi_6 = e^{6i\varphi}$, while the fluctuating fields ϑ and φ represents again the local nematic and hexatic orientations respectively. Averaging ψ_2 and ψ_6 over the scale of a volume element, yields the order complex parameters $\Psi_2 = \langle e^{2i\vartheta} \rangle = |\Psi_2|e^{2i\theta}$ and $\Psi_6 = \langle e^{6i\varphi} \rangle = |\Psi_6|e^{6i\phi}$, with θ and ϕ the average orientations. To make progress, we assume that, at the scale of a volume element, both microscopic orientations ϑ and φ are Gaussianly distributed about their mean values, so that, in general

$$\Psi_p = \langle \psi_p \rangle \approx e^{-\frac{1}{2} \text{var}[\text{Arg}(\psi_p)] + i\langle \text{Arg}(\psi_p) \rangle}, \quad (\text{S38})$$

from which

$$|\Psi_p| \approx e^{-\frac{1}{2} \text{var}[\text{Arg}(\psi_p)]}, \quad \text{Arg}(\Psi_p) = \langle \text{Arg}(\psi_p) \rangle. \quad (\text{S39})$$

This approximation holds when the relative fluctuation of the p -atic phase $\text{Arg}(\psi_p)$ is sufficiently small, so that

$$|\Psi_p| \approx 1 - \frac{1}{2} \left\langle [\text{Arg}(\psi_p) - \text{Arg}(\Psi_p)]^2 \right\rangle \approx \langle \cos [\text{Arg}(\psi_p) - \text{Arg}(\Psi_p)] \rangle, \quad (\text{S40})$$

consistent with the standard definition of p -atic order parameter. Thus, in particular, $\theta = \langle \vartheta \rangle$ and $|\Psi_2| = \langle \cos 2(\vartheta - \theta) \rangle$, whereas $\phi = \langle \varphi \rangle$ and $|\Psi_6| = \langle \cos 6(\varphi - \phi) \rangle$. This allows to write $C_{26}(\mathbf{r})$, as given by Eq. [9], in the form

$$C_{26}(\mathbf{r}) = \frac{\Psi_2(\mathbf{r})\Psi_6^*(\mathbf{0}) + \Psi_2^*(\mathbf{r})\Psi_6(\mathbf{0})}{2} e^{12[\langle \vartheta(\mathbf{r})\varphi(\mathbf{0}) \rangle - \langle \vartheta(\mathbf{r}) \rangle \langle \varphi(\mathbf{0}) \rangle]} . \quad (\text{S41})$$

At equilibrium, both nematic and hexatic order can be approximated as uniform, so that

$$\frac{\Psi_2(\mathbf{r})\Psi_6^*(\mathbf{0}) + \Psi_2^*(\mathbf{r})\Psi_6(\mathbf{0})}{2} = |\Psi_2||\Psi_6| \cos(2\theta - 6\phi) \approx \text{const} , \quad (\text{S42})$$

and the problem reduces to calculating the connected correlation function

$$C_{\vartheta\varphi}(\mathbf{r}) = \langle \vartheta(\mathbf{r})\varphi(\mathbf{0}) \rangle - \langle \vartheta(\mathbf{r}) \rangle \langle \varphi(\mathbf{0}) \rangle . \quad (\text{S43})$$

Notice that Eq. (S42) is not strictly valid for a quasi long-ranged ordered liquid crystal, where also θ and ϕ are expected to vary in space. These spatial variations, however, occur on length scales comparable with the system size and, as long as this is much larger than any of the intrinsic length scales entailed in Eqs. (2), are negligible for the purpose of this calculation. To compute $C_{\vartheta\varphi}(\mathbf{r})$, one can take the passive limit of Eqs. (2c) and linearize the resulting equations about the lowest free energy configuration. This, in turn, is determined by the sign of the constant $\chi_{2,6}$ in Eq. (6b). For $\chi_{2,6} < 0$, the hexatic and nematic directors are energetically favored to be parallel, so that $\vartheta \approx \varphi$. Conversely, when $\chi_{2,6} > 0$, the hexatic and nematic directors are preferentially tilted by $\pi/6$, hence $\vartheta = \varphi \pm \pi/6$. For presentational clarity, here we focus on the former case and, at the end of this section, we show how the same behavior holds for positive $\chi_{2,6}$ values. Thus, assuming $\chi_{2,6} < 0$ and expanding Eqs. (2c) about $\vartheta \approx \varphi$, gives

$$\partial_t \vartheta = \mathcal{D}_2 \nabla^2 \vartheta - \frac{9}{4} |\chi_2| (\vartheta - \varphi) + \xi^{(\vartheta)} , \quad (\text{S44a})$$

$$\partial_t \varphi = \mathcal{D}_6 \nabla^2 \varphi - \frac{1}{4} |\chi_6| (\varphi - \vartheta) + \xi^{(\varphi)} , \quad (\text{S44b})$$

where, as in the previous sections, we have set $\mathcal{D}_p = \Gamma_p L_p$ and $\chi_p = \Gamma_p \chi_{2,6}$ and introduced the Gaussian noise fields $\xi^{(\vartheta)}$ and $\xi^{(\varphi)}$, having vanishing mean and finite variance. Unlike the active case, however, at equilibrium the latter is related to the environmental temperature by the fluctuation-dissipation theorem. This implies

$$\langle \xi^{(\alpha)}(\mathbf{r}, t) \xi^{(\beta)}(\mathbf{r}', t') \rangle = 2k_B T \left(\frac{\delta_{\alpha\vartheta} \delta_{\beta\vartheta}}{\gamma_2} + \frac{\delta_{\alpha\varphi} \delta_{\beta\varphi}}{\gamma_6} \right) \delta(\mathbf{r} - \mathbf{r}') \delta(t - t') , \quad (\text{S45})$$

where $\gamma_p = K_p / \mathcal{D}_p$, with K_p the orientational stiffness defined in Eq. (S6), is the rotational viscosity of the associated p -atic phase. Eqs. (S44) can now be decoupled and used to compute the correlation function $C_{\vartheta\varphi}(\mathbf{r})$. For simplicity, here we set $\mathcal{D}_2 = \mathcal{D}_6 = \mathcal{D}$, $\gamma_2 = \gamma_6 = \gamma$, and $9\chi_2 = \chi_6 = 2\chi$. With this choice, taking

$$\varphi_+ = \frac{1}{2} (\varphi + \vartheta) , \quad (\text{S46a})$$

$$\varphi_- = \frac{1}{2} (\varphi - \vartheta) , \quad (\text{S46b})$$

gives, after simple algebraic manipulations

$$\partial_t \varphi_+ = \mathcal{D} \nabla^2 \varphi_+ + \xi_+ , \quad (\text{S47a})$$

$$\partial_t \varphi_- = \mathcal{D} \nabla^2 \varphi_- - |\chi| \varphi_- + \xi_- , \quad (\text{S47b})$$

where $\xi_+ = (\xi^{(\varphi)} + \xi^{(\vartheta)})/2$ and $\xi_- = (\xi^{(\varphi)} - \xi^{(\vartheta)})/2$. Moreover, using Eq. (S45), one finds

$$\langle \xi_n(\mathbf{r}, t) \xi_m(\mathbf{r}', t') \rangle = \frac{2k_B T}{\gamma} \delta_{nm} \delta(\mathbf{r} - \mathbf{r}') \delta(t - t') , \quad (\text{S48})$$

where $\{n, m\} = \{+, -\}$. Eqs. (S47) can now be solved in Fourier space and real time to give

$$\hat{\varphi}_n(\mathbf{q}, t) = e^{S_n(\mathbf{q}, t)} \left[\hat{\varphi}_n(\mathbf{q}, 0) + \int_0^t dt' e^{-S_n(\mathbf{q}, t')} \hat{\xi}_n(\mathbf{q}, t') \right] , \quad (\text{S49})$$

where the hat indicates Fourier transformation and

$$S_n(\mathbf{q}, t) = -\mathcal{D}t (|\mathbf{q}|^2 + m_n^2) , \quad (\text{S50})$$

where $m_+ = 0$ and $m_-^2 = \ell_\chi^{-2} = \mathcal{D}/|\chi|$. The calculation of the cross correlation function $C_{\partial\varphi}(\mathbf{r})$ is now reduced to calculating the autocorrelation functions of the fields φ_+ and φ_- . Specifically

$$C_{\partial\varphi}(\mathbf{r}) = C_{++}(\mathbf{r}) - C_{--}(\mathbf{r}) , \quad (\text{S51})$$

where

$$C_{nm}(\mathbf{r}) = \langle \varphi_n(\mathbf{r})\varphi_m(\mathbf{0}) \rangle - \langle \varphi_n(\mathbf{r}) \rangle \langle \varphi_m(\mathbf{0}) \rangle , \quad (\text{S52})$$

and we have made use of Eq. (S45) to demonstrate that $C_{+-}(\mathbf{r}) = C_{-+}(\mathbf{r}) = 0$. The non-vanishing correlation functions, on the other hand, can be expressed as

$$C_{nn}(\mathbf{r}) = \lim_{t \rightarrow \infty} \int_{0 < |\mathbf{q}| < \Lambda} \frac{d^2q}{(2\pi)^2} e^{i\mathbf{q}\cdot\mathbf{r}} \langle |\hat{\varphi}_n(\mathbf{q}, t)|^2 \rangle , \quad (\text{S53})$$

where $\Lambda = 2\pi/a$ is a short-distance cut-off and $\langle |\hat{\varphi}_n(\mathbf{q}, t)|^2 \rangle$ is the finite-time orientational structure factor defined from the relation

$$\langle \hat{\varphi}_n(\mathbf{q}, t)\hat{\varphi}_n(\mathbf{q}', t') \rangle = (2\pi)^2 \langle |\hat{\varphi}_n(\mathbf{q}, t)|^2 \delta(\mathbf{q} + \mathbf{q}') \delta(t - t') \rangle . \quad (\text{S54})$$

After standard algebraic manipulations one finds

$$\langle |\hat{\varphi}_n(\mathbf{q})|^2 \rangle = \lim_{t \rightarrow \infty} \langle |\hat{\varphi}_n(\mathbf{q}, t)|^2 \rangle = \frac{k_B T}{K} \frac{1}{|\mathbf{q}|^2 + m_n^2} . \quad (\text{S55})$$

from which Eq. (S53) can be calculated in the form

$$C_{nn}(\mathbf{r}) = \frac{k_B T}{K} \int_{0 < |\mathbf{q}| < \Lambda} \frac{d^2q}{(2\pi)^2} \frac{e^{i\mathbf{q}\cdot\mathbf{r}}}{|\mathbf{q}|^2 + m_n^2} . \quad (\text{S56})$$

Evidently, Eq. (S56) is equivalent to that obtained in a purely static setting from the Hamiltonian

$$\mathcal{H} = \frac{1}{2} \int d^2r [K|\nabla\varphi_+|^2 + K|\nabla\varphi_-|^2 + m_-^2\varphi_-^2] , \quad (\text{S57})$$

of the non-interacting scalar fields φ_+ and φ_- . Now, in the case of the “massive” field φ_- , the Fourier integral in Eq. (S56) converges to

$$C_{--}(\mathbf{r}) = \frac{k_B T}{2\pi K} K_0 \left(\frac{|\mathbf{r}|}{\ell_\chi} \right) , \quad (\text{S58})$$

in the range $|\mathbf{r}| \gg a$. Here K_0 is a modified Bessel function of the second kind, whose asymptotic expansion at short and long distances is given by

$$K_0(z) \approx \begin{cases} -\gamma_{\text{EM}} - \log \frac{z}{2} & 0 < z \ll 1 , \\ \sqrt{\frac{\pi}{2z}} e^{-z} & z \gg 1 \end{cases} , \quad (\text{S59})$$

with γ_{EM} the Euler-Mascheroni constant. In the case of the “massless” field φ_+ , on the other hand, the Fourier integral diverges in the infrared, but the correlation function $C_{++}(\mathbf{r})$ can still be computed as the Laplacian Green function on an infinite domain punctured by a hole of radius a at the origin. Thus

$$C_{++}(\mathbf{r}) = -\frac{k_B T}{2\pi K} \log \frac{|\mathbf{r}|}{a} . \quad (\text{S60})$$

Combining this with Eqs. (S58) and (S60) yields the following expression for the correlation function

$$C_{\partial\varphi}(\mathbf{r}) = -\frac{k_B T}{2\pi K} \left[\log \frac{|\mathbf{r}|}{a} + K_0 \left(\frac{|\mathbf{r}|}{\ell_\chi} \right) \right] , \quad (\text{S61})$$

where $|\mathbf{r}| \gg a$. Finally, using Eq. (S41) and the asymptotic expansions of Eq. (S59) gives the following expression for the cross-correlation function

$$C_{26}(\mathbf{r}) \sim \begin{cases} \text{const.} & |\mathbf{r}| \ll \ell_\chi \\ \left(\frac{|\mathbf{r}|}{a}\right)^{-\eta_{26}} & |\mathbf{r}| \gg \ell_\chi \end{cases}, \quad (\text{S62})$$

where η_{26} is an instance of the generic non-universal exponent

$$\eta_{pp'} = \frac{pp'k_B T}{2\pi K}, \quad (\text{S63})$$

in the specific case $p = 2$ and $p' = 6$. Lastly, when $\chi_{2,6} > 0$, the same procedure can be carried out by expanding Eq. (2c) about $\vartheta = \varphi \pm \pi/6$ and taking $\varphi_+ = (\varphi + \vartheta)/2$ and $\varphi_- = (\varphi - \vartheta \pm \pi/6)/2$, from which one finds again Eq. (S63).